

# **OMI measured increasing SO<sub>2</sub> emissions due to energy industry expansion and relocation in Northwestern China**

## **Authors:**

Zaili Ling<sup>1</sup>, Tao Huang<sup>1,\*</sup>, Yuan Zhao<sup>1</sup>, Jixiang Li<sup>1</sup>, Xiaodong Zhang<sup>1</sup>, Jinxiang Wang<sup>1</sup>, Lulu Lian<sup>1</sup>, Xiaoxuan Mao<sup>1</sup>, Hong Gao<sup>1</sup>, Jianmin Ma<sup>2,1,3,\*</sup>

## **Affiliations:**

<sup>1</sup>Key Laboratory for Environmental Pollution Prediction and Control, Gansu Province, College of Earth and Environmental Sciences, Lanzhou University, Lanzhou 730000, P. R. China

<sup>2</sup>Laboratory for Earth Surface Processes, College of Urban and Environmental Sciences, Peking University, Beijing, 100871, China

<sup>3</sup>CAS Center for Excellence in Tibetan Plateau Earth Sciences, Chinese Academy of Sciences, Beijing, 100101, China

**Corresponding author:** Jianmin Ma, Tao Huang

College of Earth and Environmental Sciences, Lanzhou University, 222, Tianshui South Road, Lanzhou 730000, China

Email: [jianminma@lzu.edu.cn](mailto:jianminma@lzu.edu.cn); [huangt@lzu.edu.cn](mailto:huangt@lzu.edu.cn)

1 **Abstract**

2 The rapid growth of economy makes China the largest energy consumer and sulfur  
3 dioxide (SO<sub>2</sub>) emitter in the world. In this study, we estimated the trends and step  
4 changes in the planetary boundary layer (PBL) vertical column density (VCD) of SO<sub>2</sub>  
5 from 2005 to 2015 over China measured by the Ozone Monitoring Instrument (OMI).  
6 We show that these trends and step change years coincide with the effective date and  
7 period of the national strategy for energy development and relocation in northwestern  
8 China and the regulations in the reduction of SO<sub>2</sub> emissions. Under the national  
9 regulations in the SO<sub>2</sub> emissions reduction in eastern and southern China, SO<sub>2</sub> VCD  
10 in the Pearl River Delta (PRD) of southern China exhibited the largest decline during  
11 2005-2015 at a rate of -7% yr<sup>-1</sup>, followed by the North China Plain (NCP) (-6.7% yr<sup>-1</sup>),  
12 Sichuan Basin (-6.3% yr<sup>-1</sup>), and Yangtze River Delta (YRD) (-6% yr<sup>-1</sup>), respectively.  
13 The Mann–Kendall (MK) test reveals the step change points of declining SO<sub>2</sub> VCD in  
14 2009 for the PRD and 2012-2013 for eastern China responding to the implementation  
15 of SO<sub>2</sub> control regulation in these regions. In contrast, the MK test and regression  
16 analysis also revealed increasing trends of SO<sub>2</sub> VCD in northwestern China,  
17 particularly for several "hot spots" featured by growing SO<sub>2</sub> VCD in those large-scale  
18 energy industry bases in northwestern China. The enhanced SO<sub>2</sub> VCD is potentially  
19 attributable to increasing SO<sub>2</sub> emissions due to the development of large-scale energy  
20 industry bases in energy-abundant northwestern China under the national strategy for  
21 the energy safety of China in the 21st century. We show that these large-scale energy  
22 industry bases could overwhelm the trends and changes in provincial total SO<sub>2</sub>

23 emissions in northwestern China and contributed increasingly to the national total SO<sub>2</sub>  
24 emission in China. Given that northwestern China is more ecologically fragile and  
25 uniquely susceptible to atmospheric pollution as compared with the rest of China,  
26 increasing SO<sub>2</sub> emissions in this part of China should not be overlooked and merit  
27 scientific research.

28

## 29 **1. Introduction**

30 Sulfur dioxide (SO<sub>2</sub>) is one of the criteria air pollutants emitted from both  
31 anthropogenic and natural sources. The combustions of sulfur-containing fuels, such  
32 as coal and oil, are the primary anthropogenic emitters, which contributed to the half  
33 of total SO<sub>2</sub> emissions (Smith et al., 2011; Lu et al., 2010; Stevenson et al., 2003;  
34 Whelpdale et al., 1996). With the rapid economic growth in the past decades, China  
35 has become the world's largest energy consumer accounting for 23% of global energy  
36 consumption in 2015 (BIEE, 2016). Coal has been a dominating energy source in  
37 China and accounted for 70% of total energy consumption in 2010 (Kanada et al.,  
38 2013). The huge demand for coal and its high sulfur content make China the largest  
39 SO<sub>2</sub> emission source in the world (Krotkov et al., 2016; Su et al., 2011), which also  
40 accounted for two-third of Asia's total SO<sub>2</sub> emission (Ohara et al., 2007). From 2000  
41 to 2006, the total SO<sub>2</sub> emission in China increased by 53% at an annual growth rate of  
42 7.3% (Lu et al., 2010). To reduce SO<sub>2</sub> emission, from 2005 onward the Chinese  
43 government has issued and implemented a series of regulations, strategies, and SO<sub>2</sub>  
44 control measures, leading to a drastic decrease of SO<sub>2</sub> emission, particularly in eastern

45 and southern China (Lu et al., 2011; Li et al., 2010).

46 Recently, two research groups led by NASA (National Aeronautics and Space  
47 Administration) and Lanzhou University of China published almost simultaneously  
48 the temporal and spatial trends of SO<sub>2</sub> in China from 2005 to 2015 using the OMI  
49 retrieved SO<sub>2</sub> PBL column density after the OMI is launched for 11 years (Krotkov et  
50 al., 2016; Shen et al., 2016). The results reported by the two groups revealed the  
51 widespread decline of SO<sub>2</sub> in eastern China for the past decade. Shen et al. noticed,  
52 however, that, in contrast to dramatic decreasing SO<sub>2</sub> emissions in densely populated  
53 and industrialized eastern and southern China, the OMI measured SO<sub>2</sub> in northwestern  
54 China appeared not showing a decreasing trend. This is likely resulted from the  
55 energy industry relocation and development in energy-abundant northwestern China  
56 in the past decades under the national strategy for China's energy development and  
57 safety during the 21st century. Concern is raised about the potential impact of SO<sub>2</sub>  
58 emissions on the ecological environment and health risk in northwestern China  
59 because high SO<sub>2</sub> emissions could otherwise damage the rigorous ecological  
60 environment in this part of China, featured by very low precipitation and sparse  
61 vegetation coverage which reduce considerably the atmospheric removal of air  
62 pollutants (Ma and Xu, 2017).

63 To assess and evaluate the risks of the ecological environment and public to the  
64 growing SO<sub>2</sub> emissions in northwestern China, it is necessary to investigate the  
65 spatiotemporal distributions of SO<sub>2</sub> concentrations and emissions. However, the  
66 ground measurements of ambient SO<sub>2</sub> are scarce temporally and spatially in China,

67 and often subject to significant errors and uncertainties. Owing to the rapid progress  
68 in the remote sensing techniques, satellite retrieval of air pollutants has become a  
69 powerful tool for the assessment of emissions and spatiotemporal distributions of air  
70 pollutants. In recent several years, OMI (Dutch Space, Leiden, The Netherlands,  
71 embedded on Aura satellite) retrieved SO<sub>2</sub> column concentrations have been  
72 increasingly applied to elucidate the spatiotemporal variation of global and regional  
73 SO<sub>2</sub> levels and its emissions from large point sources, and evaluate the effectiveness  
74 of SO<sub>2</sub> control policies and measures (Krotkov et al., 2016; McLinden et al., 2015,  
75 2016; Ialongo et al., 2015; Fioletov et al., 2015, 2016; Wang et al., 2015; Li et al.,  
76 2010). The decadal operation of the OMI provides the relatively long-term SO<sub>2</sub> time  
77 series data with a high spatial resolution which are particularly useful for assessing the  
78 changes and trends in SO<sub>2</sub> emissions induced by national regulations and strategies.  
79 The present study aims to (1) determine the spatiotemporal variations of SO<sub>2</sub> and its  
80 trend under the national plan for energy industry development in northwestern China  
81 by making use of the OMI-measured SO<sub>2</sub> data during 2005-2015; (2) to identify  
82 leading causes contributing to the enhanced SO<sub>2</sub> emission in northwestern China.

83

## 84 **2 Data and methods**

### 85 **2.1 Satellite data**

86 The OMI Ozone Monitoring Instrument (OMI) was launched on July 15, 2004,  
87 on the EOS Aura satellite, which is in a sun-synchronous ascending polar orbit with  
88 1:45 pm local equator crossing time. It is an ultraviolet/visible (UV/VIS) nadir solar

89 backscatter spectrometer, which provides nearly global coverage in one day, with a  
90 spatial resolution of 13 km×24 km (Levelt et al. 2006a, 2006b). It provides global  
91 measurements of ozone (O<sub>3</sub>), SO<sub>2</sub>, NO<sub>2</sub>, HCHO and other pollutants on a daily basis.  
92 The OMI uses spectral measurements between 310.5 and 340 nm in the UV-2 to  
93 detect anthropogenic SO<sub>2</sub> pollution in the lowest part of the atmosphere (Li et al.,  
94 2013). The instrument is sensitive enough to detect the near-surface SO<sub>2</sub>. Previously,  
95 the OMI PBL SO<sub>2</sub> data were produced using the Band Residual Difference (BRD)  
96 algorithm (Krotkov et al., 2006), which have large noise and unphysical biases  
97 particularly at high latitudes (Krotkov et al., 2008). Subsequently, a principal  
98 component analysis (PCA) algorithm was applied to retrieve SO<sub>2</sub> column densities.  
99 This approach greatly reduces biases and decreases the noise by a factor of 2,  
100 providing greater sensitivity to anthropogenic emissions (Li et al., 2013).

101 In the present study, we collected the level 3 OMI daily planetary boundary layer  
102 (PBL) SO<sub>2</sub> vertical column density (VCD) data in Dobson units (1 DU=2.69×10<sup>16</sup>  
103 molecules cm<sup>-2</sup>) produced by the PCA algorithm (Li et al., 2013). The spatial  
104 resolution is 0.25°×0.25° latitude/ longitude, available at Goddard Earth Sciences Data  
105 and Information Services Center  
106 ([http://disc.sci.gsfc.nasa.gov/Aura/data-holdings/OMI/omso2\\_v003.shtml](http://disc.sci.gsfc.nasa.gov/Aura/data-holdings/OMI/omso2_v003.shtml)). The systematic  
107 bias of PCA retrievals is estimated as ~0.5 DU for regions between 30°S and 30°N. The  
108 bias increases to ~0.7-0.9 DU for high latitude areas with large slant column O<sub>3</sub> but is still a  
109 factor of two smaller than that from BRD retrievals  
110 (<https://disc.gsfc.nasa.gov/Aura/data-holdings/OMI/documents/v003/omso2readme-v120-2>

111 0140926.pdf). As a result, the PCA algorithm may yield systematic errors for anthropogenic  
112 emission sources located in different latitudes and under complex topographic and  
113 underlying surface conditions. The air mass factors (AMFs) used to convert SO<sub>2</sub> slant  
114 column density (SCD) into VCD are also subject to uncertainties. Fioletov et al. (2016)  
115 revealed an overall AMF uncertainty of 28% which was created by surface reflectivity,  
116 surface pressure, ozone column, and cloud fraction. As Fioletov et al. (2016) noted, the  
117 PCA retrieved SO<sub>2</sub> VCD was virtually derived by using an AMF of 0.36 which is best  
118 applicable in the summertime in the eastern United States (US). Wang (2014) suggested  
119 adopting  $AMF \approx 0.57$  in the estimate of SO<sub>2</sub> VCD distribution in eastern China. In the  
120 present study, we have taken the AMFs values in China provided by Fioletov et al. (2016)  
121 to adjust OMI measured VCD in the estimation of the SO<sub>2</sub> emission of the main point  
122 sources in northwestern China.

## 123 **2.2 SO<sub>2</sub> monitoring, emission, and socioeconomic data**

124 To evaluate and verify the spatial SO<sub>2</sub> VCD from OMI, ground SO<sub>2</sub> monitoring  
125 data of 2014 through 2015 at 188 sampling sites (cities) across China (**Fig. 1**),  
126 operated by the National Environmental Monitoring Center, available at  
127 <http://www.aqistudy.cn/historydata>. Annually averaged SO<sub>2</sub> air concentrations from  
128 2005 to 2015 in 6 capital cities in Urumqi (Xinjiang), Yinchuan (Ningxia), Beijing  
129 (BTH and NCP), Shanghai (YRD), Guangzhou (PRD), and Chongqing (Sichuan  
130 Basin) were collected from provincial environmental bulletin published by the  
131 Ministry of Environmental Protection of China (MEPC)  
132 (<http://www.zhb.gov.cn/hjzl/zghjzkgb/gshjzkgb>. SO<sub>2</sub> anthropogenic emission

133 inventory in China with a 0.25° longitude by 0.25° latitude resolution for every two  
134 years from 2008 to 2012 was adopted from Multi resolution Emission Inventory for  
135 China (MEIC) (Li et al., 2017, available at <http://www.meicmodel.org>).

136 The socioeconomic data in China were collected from the China Statistical  
137 Yearbooks and China Energy Statistical Yearbook, published by National Bureau of  
138 Statistics of China (NBSC),  
139 (<http://www.stats.gov.cn/tjsj/ndsj/>;<http://tongji.cnki.net/kns55/Navi/HomePage.aspx?id=N2010080088&name=YCXME&floor=1>), as well as China National  
140 Environmental Protection Plan in the Eleventh Five-Years (2006-2010) and Twelfth  
141 Five-Years (2011-2015) released by MEPC (<http://www.zhb.gov.cn>). These data  
142 include industrial GDP, coal consumption, thermal power generation, steel  
143 production, and SO<sub>2</sub> emission reduction plan, and they are presented in Table 1.

### 145 **2.3 Trends and step change**

146 The long-term trends of SO<sub>2</sub> VCD were estimated by linear regressions of the  
147 gridded annually SO<sub>2</sub> VCD against their time sequence of 2005 through 2015. The  
148 gridded slopes (trends) of the linear regressions denote the increasing (positive) or  
149 decreasing (negative) rates of SO<sub>2</sub> VCD (Wang et al., 2016; Huang et al., 2015;  
150 Zhang et al., 2015, 2016).

151 The Mann-Kendall (MK) test was also employed in the assessments of the  
152 temporal trend and step change point year of SO<sub>2</sub> VCD time series. The MK test is a  
153 nonparametric statistical test (Mann,1945; Kendall, 1975), which is useful for  
154 assessing the significance of trends in time series data (Waked et al., 2016; Fathian et



155 al., 2016). The MK test is often used to detect a step change point in the long term  
 156 trend of a time series dataset (Moraes et al., 1998; Li et al., 2016; Zhao et al., 2015).  
 157 It is suitable for non-normally distributed data and censored data which are not  
 158 influenced by abnormal values (Yue and Pilon, 2004; Sharma et al. 2016; Yue and  
 159 Wang., 2004; Gao et al. 2016; Zhao et al., 2015). Recently, MK-test has also been  
 160 used in trend analysis for the time series of atmospheric chemicals, such as persistent  
 161 organic pollutants, surface ozone (O<sub>3</sub>), and non-methane hydrocarbon (Zhao et al.,  
 162 2015; Assareh et al.,2016; Waked et al.,2016; Sicard et al., 2016). Here the MK test  
 163 was used to identify the temporal variability and step change point of SO<sub>2</sub> VCD for  
 164 2005-2015 which may be associated with the implementation of the national strategy  
 165 and regulation in energy industry development and emission control during this  
 166 period. Under the null hypothesis (no trend), the test statistic was determined using  
 167 the following formula:

$$168 \quad S_k = \sum_{i=1}^k r_i \quad (k= 2, 3, \dots, n) \quad (1)$$

169 where  $S_k$  is a statistic of the MK test, and

$$170 \quad r_i = \begin{cases} +1, (x_i > x_j) \\ 0, (x_i \leq x_j) \end{cases} \quad (j=1,2, \dots, i-1) \quad (2)$$

171 where  $x_i$  is the variable in time series  $x_1, x_2, \dots, x_i$ ,  $r_i$  is the cumulative number for  
 172  $x_i > x_j$ . The test statistic is normally distributed with a mean and variance is given by:

$$173 \quad E(S_k) = k(k-1)/4 \quad (3)$$

$$174 \quad Var(S_k) = \frac{k(k-1)(2k+5)}{72} \quad (4)$$

175 From these two equations, one can derive a normalized  $S_i$ , defined by

$$176 \quad UF_k = \frac{S_k - E(S_k)}{\sqrt{Var(S_k)}} \quad (k=1, 2, \dots, n) \quad (5)$$

177 where  $UF_k$  is the forward sequence, the backward sequence  $UB_k$  is calculated using  
178 the same function but with the reverse data series such that  $UB_k = -UF_k$ .

179 In a two-sided trend test, a null hypothesis is accepted at the significance level if  
180  $|UF_k| \leq (UF_k)_{1-\alpha/2}$ , where  $(UF_k)_{1-\alpha/2}$  is the critical value of the standard normal  
181 distribution, with a probability of  $\alpha$ . When the null hypothesis is rejected (i.e., when  
182 any of the points in  $UF_k$  exceeds the confidence interval  $\pm 1.96$ ;  $P=0.05$ ), a  
183 significantly increasing or decreasing trend is determined.  $UF_k > 0$  often indicates an  
184 increasing trend and vice versa. The test statistic used in the present study enables us  
185 to discriminate the approximate time of trend and step change by locating the  
186 intersection of the  $UF_k$  and  $UB_k$  curves. The intersection occurring within the  
187 confidence interval  $(-1.96, 1.96)$  indicates the beginning of a step change point  
188 (Moraes et al., 1998; Zhang et al., 2011; Zhao et al., 2015).

#### 189 **2.4 Estimate of SO<sub>2</sub> emission from OMI measurements**

190 To assess the connections between the major point sources in large-scale energy  
191 industrial bases in northwestern China and provincial emissions, we made use of OMI  
192 measured SO<sub>2</sub> VCD to inversely simulate the SO<sub>2</sub> emission from Ningdong Energy  
193 Chemical Industrial Base (NECIB) in Ningxia and Midong Energy Industrial Base  
194 (MEIB) in Xinjiang. McLinden et al. (2016) and Fioletov et al. (2015, 2016) have  
195 developed a source detection algorithm which fits OMI-measured SO<sub>2</sub> vertical

196 column densities to a three-dimensional parameterization function of the horizontal  
 197 coordinates and wind speed. This algorithm was employed in the present study to  
 198 estimate the SO<sub>2</sub> source strength in the two industrial bases and its contribution to the  
 199 provincial total SO<sub>2</sub> emissions. The details of this algorithm are referred to Fioletov et  
 200 al (2015). Briefly, the source detection algorithm uses a Gaussian function  $f(x, y)$   
 201 multiplied by an exponentially modified Gaussian function  $g(y, s)$  to fit the OMI SO<sub>2</sub>  
 202 measurements (Fioletov et al., 2015)  $OMI_{SO_2} = a \cdot f(x, y) \cdot g(y, s)$ , defined by

$$\begin{aligned}
 f(x, y) &= \frac{1}{\sigma_1 \sqrt{2\pi}} \exp\left(-\frac{x^2}{2\sigma_1^2}\right); \\
 g(y, s) &= \frac{\lambda_1}{2} \exp\left(\frac{\lambda_1(\lambda_1\sigma^2 + 2y)}{2}\right) \cdot \operatorname{erfc}\left(\frac{\lambda_1\sigma^2 + y}{\sqrt{2}\sigma}\right); \\
 \sigma_1 &= \begin{cases} \sqrt{\sigma^2 - 1.5y}, & y < 0; \\ \sigma, & y \geq 0 \end{cases}; \\
 \lambda_1 &= \lambda / s; \\
 \operatorname{erfc}(x) &= \frac{2}{\sqrt{\pi}} \int_x^\infty e^{-t^2} dt
 \end{aligned} \tag{6}$$

204 where  $x$  and  $y$  indicate the coordinates of the OMI pixel center (km);  $s$  is the wind  
 205 speed (km h<sup>-1</sup>) at the pixel center;  $a$  represents the total number of SO<sub>2</sub> molecules (or  
 206 SO<sub>2</sub> burden) observed by OMI in a target emission source  $\lambda = 1/\tau$ , where  $\tau$  is a  
 207 decay time of SO<sub>2</sub>, and  $\sigma$  describes the width or spread of SO<sub>2</sub>.

208 The  $f(x, y)$  function represents the Gaussian distribution across the wind direction  
 209 line. The function  $g(y, s)$  represents an exponential decay along the  $y$ -axis smoothed  
 210 by a Gaussian function. Once  $\sigma$  and  $\tau$  are determined, the SO<sub>2</sub> burden as a function  
 211 of  $x, y$ , and  $s$  (OMI SO<sub>2</sub> ( $x, y, s$ )) can be reconstructed. SO<sub>2</sub> emission strength from a  
 212 large point source can be estimated by  $E = a/\tau$ . In the present study, following Fioletov

213 (2016) we choose a mean value of  $\sigma=20$  km and  $\tau=6$  h in the calculation of SO<sub>2</sub>  
214 emission large point sources of interested. Wind speed and direction on a 1°×1°  
215 latitude/longitude spatial resolution were collected from NCEP (National Centers for  
216 Environmental Prediction) Final Operational Global Analysis  
217 (<http://dss.ucar.edu/datasets/ds083.2/>). These data were interpolated to the location of  
218 each OMI pixel center on a 1/4°×1/4° latitude/longitude spacing.

219 There are several potential sources of errors which need to be taken into account  
220 when determining the overall uncertainty of the SO<sub>2</sub> emission estimation. Fioletov et  
221 al. (2016) have highlighted three primary sources of errors in the OMI-based emission  
222 estimates, including AMF, the estimation of the total SO<sub>2</sub> mass as determined from a  
223 linear regression, and the selection of  $\sigma$  and  $\tau$  used to fit OMI measurements. Based  
224 on the coefficients of variation (*CV*, %) in these three error categories (McLinden et  
225 al., 2014, 2016; Fioletov et al.; 2016) listed in **Table S1** of Supplement, we estimated  
226 uncertainties in the SO<sub>2</sub> emissions derived from OMI measurements in the two major  
227 point sources in northwestern China by running the source detection model repeatedly  
228 for 10,000 times using Monte Carlo method. Results show the standard deviation of  
229 -35 to 122 kt/yr for SO<sub>2</sub> emissions in NECIB and -29 to 95 kt/yr for SO<sub>2</sub> emissions in  
230 MEIB from 2005 to 2015, respectively.

## 231 **2.5 Satellite data validation**

232 The OMI retrieved SO<sub>2</sub> PBL VCDs were evaluated by comparing with ambient  
233 air concentration data of SO<sub>2</sub> from routine measurements by local official  
234 operational air quality monitoring stations. The statistics between OMI retrieved SO<sub>2</sub>

235 VCD and monitored annually averaged SO<sub>2</sub> air concentrations during 2014-2015 at  
236 188 operational air quality monitoring stations across China are presented in **Table**  
237 **S2** of Supplement. **Figure S1** is the correlation diagram between SO<sub>2</sub> VCD and  
238 sampled data. As shown in **Table S2** and **Fig. S1**, the OMI measured SO<sub>2</sub> VCDs  
239 agree well with the monitored ambient SO<sub>2</sub> concentrations across China at the  
240 correlation coefficient of 0.85 ( $p < 0.05$ ) (**Table S2**). **Figure 2** further compares  
241 annually averaged SO<sub>2</sub> VCD and SO<sub>2</sub> air concentrations from 2005 to 2015 in 6  
242 capital cities. These are Urumqi, Yinchuan, Beijing, Shanghai, Guangzhou, and  
243 Chongqing, respectively. The mean SO<sub>2</sub> concentration data were collected from  
244 provincial environmental bulletin published by the Ministry of Environmental  
245 Protection of China (MEPC) (<http://www.zhb.gov.cn/hjzl/zghjzkgb/gshjzkgb>).  
246 Results show that the annual variation of mean SO<sub>2</sub> VCD are higher than the  
247 measured SO<sub>2</sub> concentrations from 2010 to 2015, but SO<sub>2</sub> VCD match well with the  
248 monitored data except for Urumqi, the capital of Xinjiang Uygur Autonomous  
249 Region. The OMI retrieved SO<sub>2</sub> VCDs in Shanghai and Chongqing are higher than  
250 the measured concentrations in these two regions show consistent temporal  
251 fluctuation and trend. The measured SO<sub>2</sub> concentrations peaked in 2013 in Yinchuan  
252 whereas the SO<sub>2</sub> VCD reached the peak in 2012 and decreased thereafter. OMI  
253 measured SO<sub>2</sub> VCD in Urumqi shows different yearly fluctuations compared with its  
254 annual concentrations. The measured SO<sub>2</sub> concentrations in Urumqi decreased from  
255 2011 to 2015 whereas the OMI measured SO<sub>2</sub> VCD did not illustrate obvious  
256 changes. In particular, the monitored mean SO<sub>2</sub> concentration from 2013 to 2015

257 decreased by 75% compared with that from 2005 to 2012. This is partly attributed to  
258 the change in air quality monitoring sites in Urumqi city. Before 2013, there were  
259 only three operational air quality sites in Urumqi City, all located in the heavily  
260 polluted downtown region. Since 2013, the air monitoring sites increased from 3 to 7.  
261 The four new sites are located in less polluted suburbs of the city. As a result, the  
262 spatially averaged SO<sub>2</sub> concentrations over 3 downtown air quality monitoring sites  
263 before 2013 were higher than the mean concentrations averaged over 7 monitoring  
264 sites ([http://xjny.ts.cn/content/2012-06/05/content\\_6899388.htm](http://xjny.ts.cn/content/2012-06/05/content_6899388.htm)). It is worth noting  
265 that the measured SO<sub>2</sub> concentration in Urumqi is the highest among all cities as  
266 shown in Fig. 2 whereas the OMI VCD value in Urumqi was lower than other  
267 selected cities. This may be due to systematic biases in OMI-retrieved SO<sub>2</sub> VCD. In  
268 the present study, the level 3 OMI PBL SO<sub>2</sub> VCD data produced by the PCA  
269 retrievals were used to estimate the spatiotemporal variation in SO<sub>2</sub> pollution in  
270 China. The PCA retrievals have a negative bias over some highly reflective surfaces  
271 in arid and semi-arid lands, such as many some places in the Sahara (up to about -0.5  
272 DU in monthly mean VCD )  
273 ([https://disc.gsfc.nasa.gov/Aura/data-holdings/OMI/documents/v003/omso2readme-](https://disc.gsfc.nasa.gov/Aura/data-holdings/OMI/documents/v003/omso2readme-v120-20140926.pdf)  
274 [v120-20140926.pdf](https://disc.gsfc.nasa.gov/Aura/data-holdings/OMI/documents/v003/omso2readme-v120-20140926.pdf)). Also, PCA retrievals is subject to the systematic bias of 0.7-0.9  
275 DU in relatively high latitude regions. Located at a relatively high latitude in  
276 northwestern China with a large surrounding area covered by Gobi desert, the PCA  
277 algorithm might yield lower SO<sub>2</sub> VCD value in Urumqi than other cities shown in  
278 **Fig. 2.**

279 SO<sub>2</sub> emissions data were further collected to compare with annual OMI SO<sub>2</sub>  
280 VCD in selected regions. The results are presented in **Fig. 3**. As shown, the annual  
281 variation in SO<sub>2</sub> VCD agrees reasonably well with SO<sub>2</sub> emission data except for  
282 Urumqi-Midong region. The OMI measured SO<sub>2</sub> VCD in the PRD and Sichuan Basin  
283 decreased from 2008 to 2012, but SO<sub>2</sub> emission changed little. Compared with the  
284 other five marked regions (**Fig. 1**), the satellite measured SO<sub>2</sub> VCD in  
285 Urumqi-Midong declined in 2010 and inclined in 2012. However, SO<sub>2</sub> emissions in  
286 Urumqi-Midong 2012 are factors of 11 and 8 higher than that in 2008 and 2010,  
287 respectively. It should be noted that air pollutants released in the atmosphere are  
288 affected by physical and chemical processes. They may be transported over large  
289 distances by atmospheric motions, transformed into other compounds by chemical or  
290 photochemical processes, and "washed out" or deposited at the Earth's surface (Zhao  
291 et al., 2017; Brasseur et al., 1998). The atmospheric removal and advection processes  
292 may also contribute to the inconsistency between monitored and satellite observations.  
293 In addition, the MEIC SO<sub>2</sub> emission inventory from the bottom-up approach might be  
294 subject to large uncertainties due to data manipulation, and the lack of sufficient  
295 knowledge in human activities and emissions from different sources (Li et al., 2017;  
296 Zhao et al., 2011; Lu et al., 2011; Kurokawa et al., 2013). The uncertainties in the  
297 MEIC estimated SO<sub>2</sub> emissions used in the present study are up to ±12% (Li et al.,  
298 2017). As shown in **Fig. 3**, the OMI measured SO<sub>2</sub> VCD from 2008 to 2012 in  
299 Urumqi-Midong was about 0.2 DU which was comparable with that in the EGT.  
300 However, the reported SO<sub>2</sub> emission in Urumqi-Midong was only 4% of the SO<sub>2</sub>

301 emission in the EGT in 2012 and 0.5% of that in the EGT from 2008 to 2010. It might  
302 be subject to that part large SO<sub>2</sub> emission sources were not included in emission  
303 inventory. From this perspective, the satellite remote sensing provides a very useful  
304 tool in monitoring SO<sub>2</sub> emissions from large point sources and in the verification of  
305 emission inventories (Fioletov et al., 2015, 2016; McLinden et al., 2016; Wang et al.,  
306 2015; ).

307

### 308 **3 Results and discussion**

#### 309 **3.1. OMI measured SO<sub>2</sub> in China**

310 Given higher population density and stronger industrial activities, eastern and  
311 southern China are traditionally industrialized and heavily contaminated regions by  
312 air pollutions and acid rains caused by SO<sub>2</sub> emissions. **Figure 4a** shows annually  
313 averaged OMI SO<sub>2</sub> VCD over China on a 0.25° × 0.25° latitude/longitude  
314 resolution averaged from 2005 to 2015. SO<sub>2</sub> VCD was higher considerably in eastern  
315 and central China, and Sichuan Basin than that in northwestern China. The highest  
316 SO<sub>2</sub> VCD was found in the NCP, including Beijing-Tianjin-Hebei (BTH), Shandong,  
317 and Henan province. The annually averaged SO<sub>2</sub> VCD between 2005-2015 in this  
318 region reached 1.36 DU. This result is in line with previous satellite remote sensing  
319 retrieved SO<sub>2</sub> emissions in eastern China (Krotkov et al 2016; Lu et al., 2010;  
320 Bauduin et al., 2016; Jiang et al 2012; Yan et al., 2014). However, in contrast to the  
321 spatial distribution of decadal mean SO<sub>2</sub> VCD (**Fig. 4a**), the slopes of the linear  
322 regression relationship between annual average OMI-retrieved SO<sub>2</sub> VCD and the



323 time sequence from 2005 to 2015 over China show that the negative trends  
324 overwhelmed industrialized eastern and southern China, particularly in the NCP,  
325 Sichuan Basin, the YRD, and PRD, manifesting significant decline of SO<sub>2</sub> emissions  
326 in these regions. SO<sub>2</sub> VCD in the PRD exhibited the largest decline at a rate of 7%  
327 yr<sup>-1</sup>, followed by the NCP (6.7% yr<sup>-1</sup>), Sichuan Basin (6.3% yr<sup>-1</sup>), and the YRD (6%  
328 yr<sup>-1</sup>), respectively. Annual average SO<sub>2</sub> VCD in the PRD, NCP, Sichuan Basin, and  
329 YRD decreased by 52%, 50% , 48%, and 46% in 2015 compared to 2005 (**Fig. 5**),  
330 though the annual fluctuation of SO<sub>2</sub> VCD shows rebounds in 2007 and 2011 which  
331 are potentially associated with the economic resurgence stimulated by the central  
332 government of China (He et al., 2009; Diao et al., 2012). The reduction of SO<sub>2</sub> VCD  
333 after 2011 in these regions reflects virtually the response of SO<sub>2</sub> emissions to the  
334 regulations in the reduction of SO<sub>2</sub> release, the mandatory application of the flue-gas  
335 desulfurization (FGD) on coal-fired power plants and heavy industries, and the  
336 slowdown in the growth rate of the Chinese economy (CSC, 2011a; Wang et al.,  
337 2015, Chen et al., 2016).

338         Since in the MK test the signs and fluctuations of  $UF_k$  are often used to predict  
339 the trend of a time series, this approach is further applied to quantify the trends and  
340 step changes in annually SO<sub>2</sub> VCD time series in those highlighted regions (a-f) in  
341 **Fig. 4b** from 2005 to 2015. Results are illustrated in **Fig. 6**. As shown, the forward  
342 and backward sequences  $UF_k$  and  $UB_k$  intersect at least once from 2005 to 2015.  
343 These intersections are all well within the confidence levels between -1.96 and 1.96 at  
344 the statistical significance  $\alpha=0.01$ . A common feature of the forward sequence  $UF_k$  in

345 eastern and southern China provinces is that  $UF_k$  has been declining and become  
346 negative from 2007 to 2009 onward (**Fig. 6a-d**), confirming the downturn of  $SO_2$   
347 atmospheric emissions and levels in these industrialized and well-developed regions  
348 in China. The step change points of OMI measured  $SO_2$  VCDs in the NCP, YRD and  
349 Sichuan Basin occurred between 2012 and 2013. These step change points coincide  
350 with the implementation of the new Ambient Air Quality Standard in 2012, which set  
351 a lower ambient  $SO_2$  concentration limit in the air (MEPC, 2012), and the Air  
352 Pollution Prevention and Control Action Plan in 2013 by the State Council of China  
353 (CSC, 2013a). This Action Plan requests to take immediate actions to control and  
354 reduce air pollution in China, including cutting down industrial and mobile emission  
355 sources, adjusting industrial and energy structures, and promoting the application of  
356 clean energy in the BTH, YRD, PRD and Sichuan Basin. The step change in  $SO_2$   
357 VCD over the PRD occurred in the earlier year of 2009-2010 and from this period  
358 onward the decline of  $SO_2$  VCD speeded up, as shown by the forward sequence  $UF_k$   
359 which became negative since 2007 and was below the confidence level of -1.96 after  
360 2009, suggesting significant decreasing VCD from 2009 (**Fig. 6c**). In April 2002, the  
361 Hong Kong Special Administrative Region (HKSAR) Government and the  
362 Guangdong Provincial Government reached a consensus to reduce, on a best endeavor  
363 basis, the anthropogenic emissions of  $SO_2$  by 40% in the PRD by 2010, using 1997 as  
364 the base year  
365 ([http://www.epd.gov.hk/epd/english/action\\_blue\\_sky/files/exsummary\\_e.pdf](http://www.epd.gov.hk/epd/english/action_blue_sky/files/exsummary_e.pdf)). By the  
366 end of 2010, all thermal power units producing more than 0.125 million kilowatts

367 electricity in the PRD were equipped with the FGD. During the 11th Five-Year Plan  
368 (2006-2010), the thermal power units with 1.2 million kilowatts capacity have been  
369 shut down. SO<sub>2</sub> emission was reduced by 18% in 2010 compared to that in 2005  
370 (NBSC, 2006, 2011). This likely caused the occurrence of the step change in SO<sub>2</sub>  
371 VCD over 2009-2010.

### 372 **3.2. OMI measured SO<sub>2</sub> "hot spots" in northwestern China**

373 As also shown in **Fig. 4b**, in contrast to widespread decline of SO<sub>2</sub> VCD, there  
374 are two "hot spots" featured by moderate increasing trends of SO<sub>2</sub> VCD, located in  
375 the China's Energy Golden Triangle (EGT, Shen et al., 2016, Ma and Xu, 2017) and  
376 Urumqi-Midong region in northwestern China. The annual growth rate of SO<sub>2</sub> VCD  
377 from 2005 to 2015 are 3.4% yr<sup>-1</sup> in the EGT and 1.8% yr<sup>-1</sup> in Urumqi-Midong,  
378 respectively (**Fig. 4b**). SO<sub>2</sub> VCD in these two regions peaked in 2011 and 2013  
379 which were 1.6 and 1.7 times of that in 2005 (**Fig. 5**). The raising SO<sub>2</sub> VCD in the  
380 part of the EGT have been reported by Shen et al. (2016). The second hot spot is  
381 located in Urumqi-Midong region including MEIB that is about 40 km away from  
382 Urumqi. The both EGT and MEIB are featured by extensive coal mining, thermal  
383 power generation, coal chemical, and coal liquefaction industries. The reserve of  
384 coal, oil and natural gas in the EGT is approximately  $1.05 \times 10^{12}$  ton of standard coal  
385 equivalent, accounting for 24% of the national total energy reserve in China  
386 (CRGECCR, 2015). It has been estimated that there are deposits of 20.86 billion tons  
387 of oil, 1.03 billion cubic meters of natural gas, and 2.19 trillion tons of coal in  
388 Xinjiang, accounting for 30%, 34% and 40% of the national total (Dou, 2009). Over

389 the past decades, a large number of energy-related industries have been constructed  
390 in northwestern China, such as the EGT and MEIB to enhance China's energy  
391 security in the 21st century and speed up the local economy. The rapid development  
392 of energy and coal chemical industries in Ningxia Hui Autonomous Region and  
393 Xinjiang of northwestern China alone resulted in the significant demands to coal  
394 mining and coal products. The coal consumption, thermal power generation, and the  
395 gross industrial output increased by 2.7, 3.5, and 6.6 times in Ningxia from 2005 to  
396 2015, and by 2.7, 4.2 and 6.6 times in Xinjiang during the same period (NBSC, 2005,  
397 2015). As a result, SO<sub>2</sub> emissions increased markedly in these regions, as shown by  
398 the increasing trends of SO<sub>2</sub> VCD in the EGT and Urumqi-Midong region (**Fig. 4b**).

399 The MK forward sequence further confirms the increasing SO<sub>2</sub> VCD in the EGT  
400 and Urumqi-Midong. As seen in **Fig. 6e** and **6f**, the  $UF_k$  values for SO<sub>2</sub> VCD are  
401 positive and growing, illustrating clear upward trends of SO<sub>2</sub> VCD over these two  
402 large-scale energy industry bases, revealing the response of SO<sub>2</sub> emissions to the  
403 energy industry relocation and development in northwestern China. To guarantee the  
404 national energy security and to promote the regional economy, the EGT energy  
405 program has been accelerating since 2003 under the national energy development and  
406 relocation plan (Zhu and Ruth, 2015; Chen et al., 2016), characterized by the rapid  
407 expansion of the NECIB which is located about 40 km away from Yinchuan, the  
408 capital of Ningxia (Shen et al., 2016). By the end of 2010, a large number of coal  
409 chemical industries, including the world largest coal liquefaction and thermal power  
410 plants, have been built and operated, and the total installed capacity of thermal power

411 generating units has reached 1.47 million kilowatts (Zhao, 2016). Under the same  
412 national plan, the MEIB in Xinjiang started to construction and operation from the  
413 early to mid-2000s which have almost the same industrial structures as those in the  
414 EGT, featured by coal-fired power generation, coal chemical industry, and coal  
415 liquefaction.

416 The statistical significant step change points of SO<sub>2</sub> VCD in the EGT and  
417 Urumqi-Midong took place in 2006 and 2009 (**Fig. 6e** and **6f**), differing from those  
418 regions with decreasing trends of SO<sub>2</sub> VCD in eastern and southern China. The first  
419 step change point in 2006-2007 corresponds to the increasing SO<sub>2</sub> emissions in these  
420 two large-scale energy bases till their respective peak emissions in EGT (2007) and  
421 Urumqi-Midong (2008). The second step change point in 2009 coincides with the  
422 global financial crisis in 2008 which slowed down considerably the economic growth  
423 in 2009 in China, leading to raw material surplus and the remarkable reduction in the  
424 demand for coal products.

### 425 **3.3 OMI SO<sub>2</sub> time series and step change point year in northwestern China**

426 The clearly visible "hot spots" featured by increasing OMI measured SO<sub>2</sub> VCD  
427 in the EGT/NECIB and MEIB raise a question: to what extent could these  
428 large-scale energy industrial bases affect the trend and fluctuations of SO<sub>2</sub> emissions  
429 in northwestern China? **Figure 7** illustrates the fractions of OMI measured annual  
430 SO<sub>2</sub> VCD and SO<sub>2</sub> emissions averaged over the 6 provinces of northwestern China  
431 in the annual national total VCD (**Fig. 7a**) and emissions (**Fig. 7b**) from 2005 to  
432 2015. The both SO<sub>2</sub> VCD and emission fractions in northwestern China in the

433 national total increased over the past decade. By 2015, the mean SO<sub>2</sub> VCD fraction  
434 in 6 northwestern provinces has reached 38% in the national total. The mean  
435 emission fraction was about 20% in the national total. It should be noted that there  
436 were large uncertainties in provincial SO<sub>2</sub> emission data which often underestimated  
437 SO<sub>2</sub> emissions from major point sources (Li et al., 2017; Han et al., 2007). In this  
438 sense, OMI retrieved SO<sub>2</sub> VCD fraction provides a more reliable estimate to the  
439 contribution of SO<sub>2</sub> emission in northwestern China to the national total.

440 The annual percentage changes in SO<sub>2</sub> VCD from 2005 onward are consistent  
441 well with the per capita SO<sub>2</sub> emissions in China (**Fig. 8**). As aforementioned, while  
442 the annual total SO<sub>2</sub> emissions in the well-developed BTH, YRD, and PRD were  
443 higher than that in northwestern provinces, the per capita emissions in all provinces  
444 of northwestern China, especially in Ningxia and Xinjiang where the NECIB and  
445 MEIB are located, were about factors of 1 to 6 higher than that in the BTH, YRD,  
446 and PRD, as shown in **Fig. 8**. In contrast to declining annual emissions from the  
447 BTH, YRD, and PRD, the per capita SO<sub>2</sub> emissions in almost all western provinces  
448 have been growing from 2005 onward.

449 Since almost all large-scale coal chemical, thermal power generation, and coal  
450 liquefaction industries were built in energy-abundant and sparsely populated  
451 northwestern China over the past two decades, particularly since the early 2000s,  
452 those large-scale industrial bases in this part of China likely play an important role in  
453 the growing SO<sub>2</sub> emissions in northwestern provinces. We further examine the OMI  
454 retrieved SO<sub>2</sub> VCD to confirm and evaluate the changes in SO<sub>2</sub> emissions in

455 northwestern China which should otherwise respond to these large-scale energy  
456 programs under the national plan for energy relocation and expansion. **Figure 9**  
457 displays the MK test statistics for SO<sub>2</sub> VCD in the 6 provinces in northwestern China  
458 from 2005-2015. The forward sequence  $UF_k$  suggests decreasing trends in Shaanxi  
459 and Gansu provinces and a moderate increase in Qinghai province. In Xinjiang and  
460 Ningxia where the most energy industries were relocated and developed for the last  
461 decade (2005-2015), as aforementioned,  $UF_k$  time series estimated using SO<sub>2</sub> VCD  
462 data illustrate clear upward trends. Compared with those well-developed regions in  
463 eastern and southern China, the  $UF_k$  values of SO<sub>2</sub> VCD in these northwestern  
464 provinces are almost all positive, except for Shaanxi province where the  $UF_k$  turned  
465 to negative from 2008, and Gansu province where the  $UF_k$  value become negative  
466 during 2012-2013.

467 The step change points identified by the MK test for SO<sub>2</sub> VCD in northwestern  
468 China appear associated strongly with the development and use of coal energy. As  
469 shown in **Fig. 9**, the intersection of the forward and backward sequences  $UF_k$  and  
470  $UB_k$  within the confidence levels of -1.96 (straight green line) to 1.96 (straight  
471 purple line) can be identified in 2006 and 2007 in Ningxia and Xinjiang, respectively,  
472 corresponding well to the expansion of two largest energy industry bases from 2003  
473 onward in Ningxia (NECIB) and Xinjiang (MEIB). The step change point of SO<sub>2</sub>  
474 VCD in 2012 in Gansu province coincides with fuel-switching from coal to gas in  
475 the capital city (Lanzhou) and many other places of the province initiated from 2012  
476 (CSC, 2013b). The MK derived step change point in Shaanxi province occurred in

477 2010 which was a clear signal of marked decline of fossil fuel products in northern  
478 Shaanxi where, as the part of the EGT (Ma and Xu, 2017) of China, the largest  
479 energy industry base in the province is located, right after the global financial crisis.

480 It is interesting to note that the forward sequences  $UF_k$  of SO<sub>2</sub> VCD (**Fig. 9e** and  
481 **f**) in Ningxia and Xinjiang exhibit the similar fluctuations as that in Ningdong  
482 (NECIB) and Urumqi-Midong (MEIB) (**Fig. 9e** and **f**), manifesting the potential  
483 associations between the SO<sub>2</sub> emissions in these two large-scale energy industrial  
484 bases (major point sources) and provincial emissions in Ningxia and Xinjiang,  
485 respectively. This suggests that large-scale energy industrial bases might likely  
486 overwhelm or play an important role in the SO<sub>2</sub> emissions in those energy-abundant  
487 provinces in northwestern China. **Figure 10** illustrates mean SO<sub>2</sub> VCD from 2005 to  
488 2015 in northern Xinjiang (**Fig. 10a**) and Ningxia (**Fig. 10b**). The largest  
489 concentrations can be seen clearly in the MEIB and the NECIB in these two minority  
490 autonomous regions of China. Lower SO<sub>2</sub> concentrations are illustrated in  
491 mountainous areas of northern Xinjiang. Based on inverse modeling of SO<sub>2</sub> burdens  
492 ( $a$ , 10<sup>26</sup> molecules) in the source detection model (section 2.4), we estimated SO<sub>2</sub>  
493 emission ( $E$ , kt yr<sup>-1</sup>) in the NECIB and MEIB from 2005 to 2015, defined by  $E=a/\tau$ ,  
494 where  $\tau$  is a decay time of SO<sub>2</sub> (section 2.4). The results are illustrated in **Fig. 11**. As  
495 shown, the SO<sub>2</sub> emission increased from 2005 and reached the maximum in 2011 in  
496 the NECIB and declined thereafter, in line with the annual SO<sub>2</sub> VCD fluctuations in  
497 this energy industry base which is, as aforementioned, attributable to the economic  
498 rebound in 2011 in China. Of particular interest is the large fractions of the estimated



499 SO<sub>2</sub> emission in the NECIB in Ningxia Province (**Fig. 11a**) from 2005 to 2015.

500 These large fractions suggest that this energy industry park alone contributed up to

501 more than 50% emission to the provincial total SO<sub>2</sub> emission. Likewise, the OMI SO<sub>2</sub>

502 VCD derived SO<sub>2</sub> emissions in the MEIB also made an appreciable contribution

503 (15-20%) to the provincial total SO<sub>2</sub> emission in Xinjiang. Covered by a large area of

504 Gobi desert (Junngar Basin), there are only a few of SO<sub>2</sub> emission sources in vast

505 northern Xinjiang region (total area of Xinjiang is  $1.66 \times 10^6$  km<sup>2</sup>). This likely leads to

506 the small fractions of SO<sub>2</sub> emissions in the MEIB in the total SO<sub>2</sub> emission in

507 Xinjiang. **Figure 11c** and **11d** show SO<sub>2</sub> VCDs (the left y-axis) and the ratios (the

508 right y-axis) of the mean VCDs in NECIB and MEIB to the provincial mean VCDs in

509 Ningxia and Xinjiang from 2005 to 2015, respectively. It can be seen that the

510 maximum mean SO<sub>2</sub> VCD over the MEIB is about a factor of 4.5 greater than the

511 mean SO<sub>2</sub> VCD over Xinjiang province (**Fig. 11d**). This ratio is larger than the ratio

512 (2.9) of the SO<sub>2</sub> VCD in the NECIB to the SO<sub>2</sub> VCD averaged over Ningxia province

513 (**Fig. 11c**). Nevertheless, overall our results manifest that, although there were only a

514 small number of SO<sub>2</sub> point sources in these two energy industrial bases, the SO<sub>2</sub>

515 emissions from the NECIB and MEIB made significant contributions to provincial

516 total emissions. Given that the national strategy for China's energy expansion and

517 safety during the 21st century is, to a large extent, to develop large-scale energy

518 industry bases in northwestern China, particularly in Xinjiang and Ningxia (Zhu and

519 Ruth, 2015; Chen et al., 2016) where the energy resources are most abundant in China,

520 we would expect that the rising SO<sub>2</sub> emissions in northwestern China would

521 increasingly be attributed to those large-scale energy industry bases and contributed to  
522 the national total SO<sub>2</sub> emission in China.

523 **Table 1** presents the annual average growth rates of SO<sub>2</sub> VCD, industrial  
524 (second) Gross Domestic Product (GDP), and major coal-consuming industries in  
525 northwestern China and three developed areas (BTH, YRD, PRD) in eastern and  
526 southern China. The positive growth rates of SO<sub>2</sub> VCD can be observed in the three  
527 provinces and autonomous regions (Qinghai, Ningxia, and Xinjiang) of northwestern  
528 China. Although the growth rates of SO<sub>2</sub> VCD in other two provinces (Gansu and  
529 Shaanxi) are negative, the magnitudes of the negative growth rates are smaller than  
530 those in the BTH, YRD, and PRD, except for Zhejiang province in the YRD. This  
531 regional contrast reflects both their economic and energy development activities and  
532 the SO<sub>2</sub> emission control measures implemented by the local and central  
533 governments of China. Although China has set a national target of 10% SO<sub>2</sub>  
534 emission reduction (relative to 2005) during 2006-2010 and 8% (relative to 2010)  
535 during 2011-2015 (CSC, 2007; CSC, 2011b), under the Grand Western Development  
536 Program of China, the regulation for SO<sub>2</sub> emission control was waived in those  
537 energy-abundant provinces of northwestern China in order to speed up the  
538 large-scale energy industrial bases and local economic development, and improve  
539 local personal income. Also, although FGDs were widely installed in coal-fired  
540 power plants and other industrial sectors since the 1990s, by 2010 as much as 57%  
541 of these systems were installed in eastern and southern China (Zhao et al., 2013).  
542 The capacity of small power generators which were shut-down in western China was

543 merely about 10808 MW, only accounting for about 19% of the capacity of total  
544 small power plants which were eliminated in China (55630 MW) during the 11th  
545 Five-Year Plan period (2006-2010) (Cui et al., 2016). As shown in **Table 1**, the SO<sub>2</sub>  
546 emission reduction plans virtually specified the zero percentage of SO<sub>2</sub> emission  
547 reductions in Qinghai, Gansu, and Xinjiang and lower reduction percentage in the  
548 emission reduction in Ningxia and Inner Mongolia as compared to eastern and  
549 southern China during the 11th (2006-2010) and 12th (2011-2015) Five-Year Plan.  
550 As a result, the average growth rate for thermal power generation, steel production,  
551 and coal consumption from 2005 to 2015 in northwestern China reached 14.1% yr<sup>-1</sup>,  
552 35.7% yr<sup>-1</sup>, and 11.9% yr<sup>-1</sup>, considerably higher than the averaged growth rates over  
553 eastern and southern China (5.9% yr<sup>-1</sup> in the BTH, 0.8% yr<sup>-1</sup> in the YRD, and 2.3%  
554 yr<sup>-1</sup> in the PRD).

#### 555 **4 Conclusions**

556 The spatiotemporal variation in SO<sub>2</sub> concentration during 2005-2015 over  
557 China was investigated by making use of the PBL SO<sub>2</sub> column concentrations  
558 measured by the OMI. The highest SO<sub>2</sub> VCD was found in the NCP, the most  
559 heavily polluted area by SO<sub>2</sub> in China, including Beijing-Tianjin-Hebei, Shandong,  
560 and Henan province. Under the national regulation for SO<sub>2</sub> control and emission  
561 reduction, the SO<sub>2</sub> VCD in eastern and southern China underwent widespread  
562 decline during this period. However, the OMI measured SO<sub>2</sub> VCD detected two "hot  
563 spots" in the EGT (Ningxia-Shaanxi-Inner Mongolia) and Midong (Xinjiang) energy  
564 industrial bases, in contrast to the declining SO<sub>2</sub> emissions in eastern and southern

565 China, displaying an increasing trend with the annual growth rate of 3.4% yr<sup>-1</sup> in the  
566 EGT and 1.8% yr<sup>-1</sup> in Midong, respectively. The trend analysis further revealed  
567 enhanced SO<sub>2</sub> emissions in most provinces of northwestern China likely due to the  
568 national strategy for energy industry expansion and relocation in energy-abundant  
569 northwestern China. As a result, per capita SO<sub>2</sub> emission in northwestern China has  
570 exceeded industrialized and populated eastern and southern China, making  
571 increasing contributions to the national total SO<sub>2</sub> emission. The estimated SO<sub>2</sub>  
572 emissions in the Ningdong (Ningxia) and Midong (Xinjiang) energy industrial bases  
573 from OMI measured SO<sub>2</sub> VCD showed that the SO<sub>2</sub> emissions in these two industrial  
574 bases made significant contributions to the total provincial emissions. This indicates,  
575 on one side, that the growing SO<sub>2</sub> emissions in northwestern China would  
576 increasingly come from those large scale energy industrial bases under the national  
577 energy development and relocation plan. On the other side, this fact also suggests  
578 that it is likely more straightforward to control and reduce SO<sub>2</sub> emissions in  
579 northwestern China because the SO<sub>2</sub> control measures could be readily implemented  
580 and authorized in those state-owned large-scale energy industrial bases.

581

582 **The Supplement related to this article is available online**

583 *Acknowledgements.* This work is supported by the National Natural Science  
584 Foundation of China (grants 41503089, 41371478, and 41671460), Gansu Province  
585 Science and Technology Program for Livelihood of the People (1503FCMA003), the  
586 Natural Science Foundation of Gansu Province of China (1506RJZA212), and

587 Fundamental Research Funds for the Central Universities (lzujbky-2016-249 and  
588 lzujbky-2016-253). We thank Dr. Vitali Fioletov for his suggestions and advice  
589 during the preparation of this manuscript.

590

## 591 **Reference**

592 Assareh, N., Prabamroong, T., Manomaiphiboon, K., Theramongkol, P., Leungsakul,  
593 S., Mitrijit, N., and Rachiwong, J.: Analysis of observed surface ozone in the dry  
594 season over Eastern Thailand during 1997–2012, *Atmos. Res.*, 178, 17-30, doi:  
595 10.1016/j.atmosres.2016.03.009, 2016.

596 Bauduin, S., Clarisse, L., Hadji-Lazaro, J., Theys, N., Clerbaux, C., and Coheur, P. F.:  
597 Retrieval of near-surface sulfur dioxide (SO<sub>2</sub>) concentrations at a global scale  
598 using IASI satellite observations, *Atmos. Meas. Tech.*, 9, 721-740, doi:  
599 10.5194/amt-9-721-2016, 2016.

600 BIEE (British Institute of Energy Economics): BP Statistical Review of World  
601 Energy June 2016, Available at:  
602 <http://www.bp.com/content/dam/bp/pdf/energy-economics/statistical-review-2016>  
603 </bp-statistical-review-of-world-energy-2016-full-report.pdf> (last access: 21  
604 January 2017 ), 2016.

605 Brasseur, G. P., Hauglustaine, D. A., Walters, S., Rasch, P. J., Müller, J. F., Granier,  
606 C., and Tie, X. X.: MOZART, a global chemical transport model for ozone and  
607 related chemical tracers: 1. Model description, *J Geophys. Res.*, 103,  
608 28265–28289, doi: 10.1029/98JD02397, 1998.

609 Chen, J., Cheng, S., Song, M., and Wang, J.: Interregional differences of coal carbon  
610 dioxide emissions in China, *Energ. Policy*, 96, 1–13, doi:  
611 10.1016/j.enpol.2016.05.015, 2016.

612 CRGECR (The Comprehensive Research Group for Energy Consulting and  
613 Research): Strategy on the Development of Energy “Golden Triangle”,  
614 *Engineering Science.*, 9, 18-28, 2015 (in Chinese).

615 CSC (China's State Council): China National Environmental Protection Plan in the  
616 11th Five-year (2006-2010), Available at:  
617 [http://www.gov.cn/zwggk/2007-11/26/content\\_815498.htm](http://www.gov.cn/zwggk/2007-11/26/content_815498.htm) (last access: 21 January  
618 2017), 2007 (in Chinese).

619 CSC (China's State Council): Circular on accelerating the number of comments on  
620 shutting down small thermal power units in China, Available at  
621 [http://www.gov.cn/zwggk/2007-01/26/content\\_509911.htm](http://www.gov.cn/zwggk/2007-01/26/content_509911.htm) (last access: 21 January  
622 2017 ), 2011a (in Chinese).

623 CSC (China's State Council): China National Environmental Protection Plan in the  
624 12th Five-year (2011-2015), Available at:  
625 [http://www.gov.cn/zwggk/2011-12/20/content\\_2024895.htm](http://www.gov.cn/zwggk/2011-12/20/content_2024895.htm) (last access: 21  
626 January 2017), 2011b (in Chinese).

627 CSC (China's State Council): Air Pollution Prevention and Control Action Plan,  
628 Available at: [http://www.gov.cn/zhengce/content/2013-09/13/content\\_4561.htm](http://www.gov.cn/zhengce/content/2013-09/13/content_4561.htm)  
629 (last access: 21 January 2017 ), 2013a (in Chinese).

630 CSC (China's State Council): Determination, Measures and Strength-Lanzhou

631 pollution control reproduce the blue sky, Available at:  
632 [http://www.gov.cn/jrzq/2013-02/03/content\\_2325835.htm](http://www.gov.cn/jrzq/2013-02/03/content_2325835.htm) (last access: 21 January  
633 2017), 2013b (in Chinese).

634 Cui, Y., Lin, J., Song, C., Liu, M., Yan, Y., Xu, Y., and Huang, B.: Rapid growth in  
635 nitrogen dioxide pollution over Western China, 2005-2013. *Atmos. Chem. Phys.*,  
636 16, 6207-6221, doi: 10.5194/acp-16-6207-2016, 2016.

637 Diao, X., Zhang, Y., and Chen, K. Z.: The global recession and China's stimulus  
638 package: A general equilibrium assessment of country level impacts, *China. Econ.*  
639 *Rev.*, 23, 1-17, doi: 10.1016/j.chieco.2011.05.005, 2012.

640 Dou, L.: A research on the impact of industrialization on the environment in  
641 Xinjiang with an empirical analysis, Mater thesis, Xinjiang University, Urumqi,  
642 2009 (in Chinese).

643 Fathian, F., Dehghan, Z., Bazrkar, M. H., and Eslamian, S.: Trends in hydrological  
644 and climatic variables affected by four variations of the Mann-Kendall approach  
645 in Urmia Lake Basin, Iran. *Hydrolog. Sci. J.*, 61, 892-904, doi:  
646 10.1080/02626667.2014.932911, 2016.

647 Fioletov, V. E., McLinden, C. A., Krotkov, N., and Li, C.: Lifetimes and emissions of  
648 SO<sub>2</sub> from point sources estimated from OMI, *Geophys. Res. Lett.*, 42, 1969-1976,  
649 doi: 10.1002/2015GL063148, 2015.

650 Fioletov, V. E., McLinden, C. A., Krotkov, N., Li, C., Joiner, J., Theys, N., Carn, S.,  
651 and Moran, M. D.: A global catalogue of large SO<sub>2</sub> sources and emissions derived  
652 from the Ozone Monitoring Instrument, *Atmos. Chem. Phys.*, 16, 11497–11519,

653 doi: 10.5194/acp-16-11497-2016, 2016.

654 Gao, T., and Shi, X.: Spatio-temporal characteristics of extreme precipitation events  
655 during 1951-2011 in Shandong, China and possible connection to the large scale  
656 atmospheric circulation, *Stoch. Env. Res. Risk. A.*, 30, 1421-1440, doi:  
657 10.1007/s00477-015-1149-7, 2016.

658 Han, Y.; Gao, J.; Li, H; and Li, Y.: Ecological suitability analysis on the industry  
659 overall arrangement plan of Ningdong energy sources and chemical industry base,  
660 *Environ. Sci. Manager*, 32, 142-147,2007 (in Chinese).

661 He, D., Zhang, Z., and Zhang, W.: How large will be the effect of China's fiscal  
662 stimulus package on output and employment, *Pacific Economic Review*, 14,  
663 730-744, doi: 10.1111/j.1468-0106.2009.00480.x, 2009.

664 Huang, T., Jiang, W., Ling, Z., Zhao, Y., Gao, H., and Ma, J.: Trend of cancer risk of  
665 Chinese inhabitants to dioxins due to changes in dietary patterns 1980-2009, *Sci.*  
666 *Rep.*, 6, doi: 10.1038/srep21997, 2016.

667 Ialongo, I., Hakkarainen, J., Kivi, R., Anttila, P., Krotkov, N. A., Yang, K., Li, C.,  
668 Tukiainen, S., Hassinen, S., and Tamminen, J.: Comparison of operational  
669 satellite SO<sub>2</sub> products with ground-based observations in northern Finland during  
670 the Icelandic Holuhraun fissure eruption, *Atmos. Meas. Tech.*, 8, 2279-2289, doi:  
671 10.5194/amt-8-2279-2015, 2015.

672 Jiang, J., Zha, Y., Gao, J., and Jiang, J.: Monitoring of SO<sub>2</sub> column concentration  
673 change over China from Aura OMI data, *Int. J. Remote Sen.*, 33, 1934-1942, doi:  
674 10.1080/01431161.2011.603380, 2012.



675 Kanada, M., Dong, L., Fujita, T., Fujita, M., Inoue, T., Hirano, Y., Togawa, T., and  
676 Geng, Y.: Regional disparity and cost-effective SO<sub>2</sub> pollution control in China: A  
677 case study in 5 mega-cities, *Energ. Policy*, 61, 1322-1331,  
678 doi:10.1016/j.enpol.2013.05.105, 2013.

679 Kendall, M. G., and Charles, G.: Rank correlation methods, Oxford Univ. Press,  
680 New York., USA, 202 pp., 1975.

681 Krotkov, N. A., Carn, S. A., Krueger, A. J., Bhartia, P. K., and Yang, K.: Band  
682 Residual Difference Algorithm for Retrieval of SO<sub>2</sub> From the Aura Ozone  
683 Monitoring Instrument (OMI), *IEEE T. Geosci. Remote*, 44, 1259-1266,  
684 doi:10.1109/TGRS.2005.861932, 2006.

685 Krotkov, N. A., McClure, B., Dickerson, R. R., Carn, S. A., Li, C., Bhartia, P. K.,  
686 Yang, K., Krueger, A. J., Li, Z., Levelt, P. F., Chen, H., Wang, P., and Lu, D.:  
687 Validation of SO<sub>2</sub> retrievals from the Ozone Monitoring Instrument over NE  
688 China, *J. Geophys. Res.*, 113, D16S40, doi:10.1029/2007JD008818, 2008.

689 Krotkov, N. A., McLinden, C. A., Li, C., Lamsal, L. N., Celarier, E. A., Marchenko,  
690 S. V., Swartz, W. H., Bucsela, E. J., Joiner, J., Duncan, B. N., Boersma, K. F.,  
691 Veefkind, J. P., Levelt, P. F., Fioletov, V. E., Dickerson, R. R., He, H., Lu, Z., and  
692 Streets, D. G.: Aura OMI observations of regional SO<sub>2</sub> and NO<sub>2</sub> pollution changes  
693 from 2005 to 2015, *Atmos. Chem. Phys.*, 16, 4605-4629, doi:  
694 10.5194/acp-16-4605-2016, 2016.

695 Kurokawa, J., Ohara, T., Morikawa, T., Hanayama, S., Greet, J. M., G., Fukui, T.,  
696 Kawashima, K., and Akimoto, H.: Emissions of air pollutants and greenhouse

697 gases over Asian regions during 2000–2008: Regional Emission Inventory in Asia  
698 (REAS) version 2, *Atmos. Chem. Phys.*, 13, 11019–11058, doi:  
699 10.5194/acp-13-11019-2013, 2013.

700 Levelt, P. F., Van der Oord, G. H. J., Dobber, M. R., Malkki, A., Visser, H., De Vries,  
701 J., Stammes, P., Lundell, J., Saari, H.: The ozone monitoring instrument. *IEEE*  
702 *Transactions on Geoscience and Remote Sensing*, 44, 1093-1101,  
703 doi:10.1109/TGRS.2006.872333, 2006a.

704 Levelt, P. F., Hilsenrath, E., Leppelmeier, G. W., Oord, G. H. J. Van Den, Bhartia, P.  
705 K., Tamminen, J., De Haan, J. F., and Veefkind, J. P.: Science Objectives of the  
706 Ozone Monitoring Instrument, *IEEE T. Geosci. Remote Sens.*, 44, 1199-1208,  
707 2006b.

708 Li, C., Joiner, J., Krotkov, N. A., and Bhartia, P. K.: A fast and sensitive new satellite  
709 SO<sub>2</sub> retrieval algorithm based on principal component analysis: Application to the  
710 Ozone Monitoring Instrument, *Geophys. Res. Lett.*, 40, 6314-6318, doi:  
711 10.1002/2013GL058134, 2013.

712 Li, C., Wang, R., Ning, H., and Luo, Q.: Changes in climate extremes and their  
713 impact on wheat yield in Tianshan Mountains region, northwest China, *Environ.*  
714 *Earth Sci.*, 75, doi: 10.1007/s12665-016-6030-6, 2016.

715 Li, C., Zhang, Q., Krotkov, N. A., Streets, D. G., He, K., Tsay, S. C., and Gleason, J.  
716 F.: Recent large reduction in sulfur dioxide emissions from Chinese power plants  
717 observed by the Ozone Monitoring Instrument, *Geophys. Res. Lett.*, 37, L08807,  
718 doi: 10.1029/2010GL042594, 2010.

719 Li, M., Zhang, Q., Kurokawa, J., Woo, J., He, K., Lu, Z., Ohara, T., Song, Y., Streets,  
720 D. G., Carmichael, G. R., Cheng, Y., Hong, C., Huo, H., Jiang, X., Kang, S., Liu,  
721 F., Su, H., and Zheng, B.: MIX: a mosaic Asian anthropogenic emission inventory  
722 under the international collaboration framework of the MICS-Asia and HTAP,  
723 *Atmos. Chem. Phys.*, 17, 935-963, doi: 10.5194/acp-17-935-2017, 2017.

724 Lu, Z., Streets, D. G., Zhang, Q., Wang, S., Carmichael, G. R., Cheng, Y. F., Wei, C.,  
725 Chin, M., Diehl, T., and Tan, Q.: Sulfur dioxide emissions in China and sulfur  
726 trends in East Asia since 2000, *Atmos. Chem. Phys.*, 10, 6311-6331, doi:  
727 10.5194/acp-10-6311-2010, 2010.

728 Lu, Z., Zhang, Q., and Streets, D. G.: Sulfur dioxide and primary carbonaceous  
729 aerosol emissions in China and India, 1996-2010, *Atmos. Chem. Phys.*, 11,  
730 9839-9864, doi: 10.5194/acp-11-9839-2011, 2011.

731 Ma, J., and Xu, J.: China's energy rush harming ecosystem, *Nature*, 541-30, doi:  
732 10.1038/541030b, 2017.

733 Mann, H. B.: Nonparametric tests against trend, *Econometrica*, 13, 245-259, doi:  
734 10.2307/1907187, 1945.

735 McLinden, C. A., Fioletov, V., Boersma, K. F., Kharol, S. K., Krotkov, N., Lamsal,  
736 L., Makar, P. A., Martin, R. V., Veefkind, J. P., and Yang, K.: Improved satellite  
737 retrievals of NO<sub>2</sub> and SO<sub>2</sub> over the Canadian oil sands and comparisons with  
738 surface measurements, *Atmos. Chem. Phys.*, 14, 3637-3656,  
739 doi:10.5194/acp-14-3637-2014, 2014.

740 McLinden, C. A., Fioletov, V., Krotkov, N. A., Li, C., Boersma, K. F., and Adams, C.:

741 A decade of change in NO<sub>2</sub> and SO<sub>2</sub> over the Canadian oil sands as seen from  
742 space, *Environ. Sci. Technol.*, 50, 331-337, doi: 10.1021/acs.est.5b04985, 2015.

743 McLinden, C. A., Fioletov, V., Shephard, M. W., Krotkov, N., Li, C., Martin, R. V.,  
744 Moran, M. D., and Joiner, J.: Space-based detection of missing sulfur dioxide  
745 sources of global air pollution, *Nature Geosci.*, 9, 496-500, doi: 10.1038/ngeo2724,  
746 2016.

747 MEPC (Ministry of Environmental Protection of China): Ambient air quality  
748 standards, Available at:  
749 [http://kjs.mep.gov.cn/hjbhzb/bzwb/dqhjbh/dqhjzlbz/201203/t20120302\\_224165.s](http://kjs.mep.gov.cn/hjbhzb/bzwb/dqhjbh/dqhjzlbz/201203/t20120302_224165.shtml)  
750 [html](http://kjs.mep.gov.cn/hjbhzb/bzwb/dqhjbh/dqhjzlbz/201203/t20120302_224165.shtml) (last access:21 January 2017 ), 2012 (in Chinese).

751 Moraes, J. M., Pellegrino, G. Q., Ballester, M. V., Martinelli, L. A., Victoria, R. L.,  
752 and Krusche, A. V.: Trends in hydrological parameters of a southern Brazilian  
753 watershed and its relation to human induced changes, *Water Resour. Manag.*, 12,  
754 295-311, doi: 10.1023/A:1008048212420, 1998.

755 NBSC(National Bureau of Statistics of China): China Energy Statistical Yearbook  
756 2005, China Statistics Press, Beijing, 2005.

757 NBSC(National Bureau of Statistics of China): China Energy Statistical Yearbook  
758 2006, China Statistics Press, Beijing, 2006.

759 NBSC(National Bureau of Statistics of China): China Energy Statistical Yearbook  
760 2011, China Statistics Press, Beijing, 2011.

761 NBSC(National Bureau of Statistics of China): China Energy Statistical Yearbook  
762 2015, China Statistics Press, Beijing, 2015.

763 Ohara, T., Akimoto, H., Kurokawa, J., Horii, N., Yamaji, K., Yan, X., and Hayasaka,  
764 T.: An Asian emission inventory of anthropogenic emission sources for the period  
765 1980–2020, *Atmos. Chem. Phys.*, 7, 4419-4444, doi: 10.5194/acp-7-4419-2007,  
766 2007.

767 Sharma, C. S., Panda, S. N., Pradhan, R. P., Singh, A., and Kawamura, A.:  
768 Precipitation and temperature changes in eastern India by multiple trend detection  
769 methods, *Atmos. Res.*, 180, 211-225, doi: 10.1016/j.atmosres.2016.04.019,  
770 2016.

771 Shen, Y., Zhang, X., Brook, J. R., Huang, T., Zhao, Y., Gao, H., and Ma, J.: Satellite  
772 remote sensing of air quality in the Energy Golden Triangle in Northwest China,  
773 *Environ. Sci. Technol. Lett.*, 3,275-279, doi: 10.1021/acs.estlett.6b00182, 2016.

774 Sicard, P., Serra, R., and Rossello, P.: Spatiotemporal trends in ground-level ozone  
775 concentrations and metrics in France over the time period 1999-2012, *Environ.*  
776 *Res.*, 149, 122-144, doi:10.1016/j.envres.2016.05.014, 2016.

777 Smith, S. J., van Aardenne, J., Klimont, Z., Andres, R. J., Volke, A., and Delgado  
778 Arias, S.: Anthropogenic sulfur dioxide emissions: 1850-2005, *Atmos. Chem.*  
779 *Phys.*, 11, 1101-1116,doi:10.5194/acp-11-1101-2011, 2011.

780 Stevenson, D. S., Johnson, C. E., Collins, W. J., and Derwent, R. G.: The atmospheric  
781 sulphur cycle and the role of volcanic SO<sub>2</sub>, *Geol. Soc. Lond. Spec. Publ.*, 213,  
782 295-305, doi: 10.1144/GSL.SP.2003.213.01.18, 2003.

783 Su, S., Li, B., Cui, S., and Tao, S.: Sulfur Dioxide Emissions from Combustion in  
784 China: From 1990 to 2007, *Environ. Sci. Technol.*, 45, 8403-8410, doi:

785 10.1021/es201656f, 2011.

786 Waked, A., Sauvage, S., Borbon, A., Gauduin, J., Pallares, C., Vagnet, M. P., Thierry,  
787 L., and Locoge, N.: Multi-year levels and trends of non-methane hydrocarbon  
788 concentrations observed in ambient air in France, *Atmos. Environ.*, 141, 263-275,  
789 doi: 10.1016/j.atmosenv.2016.06.059, 2016.

790 Wang, S., Zhang, Q., Martin, R.V., Philip, S., Liu, F., Li, M., Jiang, X., and He, K.:  
791 Satellite measurements oversee China's sulfur dioxide emission reductions from  
792 coal-fired power plants, *Environ. Res. Lett.*, 10, 114015, doi:  
793 10.1088/1748-9326/10/11/114015, 2015.

794 Wang, S., Satellite remote sensing of the sulfur dioxide and nitrogen dioxide  
795 emissions from coal-fired power plants, PhD thesis, Tsinghua University, Beijing,  
796 2014.

797 Wang, Z., Shao, M., Chen, L., Tao, M., Zhong, L., Chen, D., Fan, M., Wang, Y., and  
798 Wang, X.: Space view of the decadal variation for typical air pollutants in the  
799 Pearl River Delta (PRD) region in China, *Front. Env. Sci. Eng.*, 10, doi:  
800 10.1007/s11783-016-0853-y, 2016.

801 Whelpdale, D. M., Dorling, S. R., Hicks, B. B., and Summers, P.W.: Atmospheric  
802 process in: *Global Acid Deposition Assessment*, edited by: Whelpdale, D. M., and  
803 Kaiser, M. S., World Meteorological Organization Global Atmosphere Watch,  
804 Report Number 106, Geneva, 7-32, 1996.

805 Yan, H., Chen, L., Su, L., Tao, J., and Yu, C.: SO<sub>2</sub> columns over China: Temporal  
806 and spatial variations using OMI and GOME-2 observations, 35th International

807 Symposium on Remote Sensing of Environment, 17, 012027, doi:  
808 10.1088/1755-1315/17/1/012027, 2014.

809 Yue, S and Pilon, P.: A comparison of the power of the t-test, Mann-Kendall and  
810 bootstrap tests for trend detection, *Hydrolog. Sci. J.*, 49, 21-37, doi:  
811 10.1623/hysj.49.1.21.53996, 2004.

812 Yue, S., and Wang, C.: The Mann-Kendall test modified by effective sample size to  
813 detect trend in serially correlated hydrological series, *Water Resour. Manag.*, 18,  
814 201-218, doi: 10.1023/B:WARM.0000043140.61082.60, 2004.

815 Zhang, X., Huang, T., Zhang, L., Gao, H., Shen, Y., and Ma, J.: Trends of deposition  
816 fluxes and loadings of sulfur dioxide and nitrogen oxides in the artificial Three  
817 Northern Regions Shelter Forest across northern China, *Environ. Pollut.*, 207, doi:  
818 10.1016/j.envpol.2015.09.022 238-247, 2015.

819 Zhang, X., Huang, T. Zhang, L., Shen, Y., Zhao, Y., Gao, H., Mao, X., Jia, C., and  
820 Ma, J.: Three-North Shelter Forest Program contribution to long-term increasing  
821 trends of biogenic isoprene emissions in northern China, *Atmos. Chem. Phys.*, 16,  
822 6949-6960, doi: 10.5194/acp-16-6949-2016, 2016.

823 Zhang, Y., Guan, D., Jin, C., Wang, A., Wu, J., and Yuan, F.: Analysis of impacts of  
824 climate variability and human activity on stream flow for a river basin in  
825 northeast China, *J. Hydrol.*, 410, 239-247, doi: 10.1016/j.jhydrol.2011.09.023,  
826 2011.

827 Zhao, B., Wang, S. X., Liu, H., Xu, J. Y., Fu, K., Klimont, Z., Hao, J. M., He, K. B.,  
828 Cofala, J., and Amann, M.: NO<sub>x</sub> emissions in China: historical trends and future

829 perspectives, *Atmos. Chem. Phys.*, 13, 9869–9897, doi:  
830 10.5194/acp-13-9869-2013, 2013.

831 Zhao, H., Li, X., Zhang, Q., Jiang, X., Lin, J., Peters, G. G., Li, M., Geng, G., Zheng,  
832 B., Huo, H., Zhang, L., Davis, S. J., and He, K.: Effects of atmospheric transport  
833 and trade on air pollution mortality in China, *Atmos. Chem. Phys. Discuss.*,  
834 doi:10.5194/acp-2017-263, in review, 2017.

835 Zhao, L.: Strategic thinking on construction of Ningdong Energy Chemical Base and  
836 development of Ningxia Coal Industry Group, *Northwest Coal*, 4, 11-13, 2016 (in  
837 Chinese).

838 Zhao, Y., Huang, T., Wang, L., Gao, H., and Ma, J.: Step changes in persistent  
839 organic pollutants over the Arctic and their implications, *Atmos. Chem. Phys.*, 15,  
840 3479-3495, doi: 10.5194/acp-15-3479-2015, 2015.

841 Zhao, Y., Nielsen, C. P., Lei, Y., McElroy, M. B., and Hao, J.: Quantifying the  
842 uncertainties of a bottom-up emission inventory of anthropogenic atmospheric  
843 pollutants in China, *Atmos. Chem. Phys.*, 11, 2295–2308, doi:  
844 10.5194/acp-11-2295-2011, 2011.

845 Zhu, J.; and Ruth, M.: Relocation or reallocation: Impacts of differentiated energy  
846 saving regulation on manufacturing industries in China, *Ecol. Econ.*, 110,  
847 119–133, doi: 10.1016/j.ecolecon.2014.12.020, 2015.

848  
849  
850  
851 **Table 1** Annual growth rate for OMI SO<sub>2</sub> VCD and economic activities for



852 individual provinces and municipality during 2005-2014 (% yr<sup>-1</sup>), and SO<sub>2</sub> emission  
 853 reduction plan during the 11th and 12th Five-Year Plan period (%).

Region	OMI SO <sub>2</sub> VCD	coal consumption	Industrial GDP	Thermal power generation	steel production	SO <sub>2</sub> emission reduction plan (%)		
						2006-2010 <sup>a</sup>	2011-2015 <sup>b</sup>	
Northwest em	Inner Mongolia	0.94	11.29	20.48	14.07	8.38	-3.8	-3.8
	Shaanxi	-3.41	13.14	19.96	13.01	14.48	-12	-7.9
	Gansu	-0.09	6.69	14.19	8.89	9.92	0	2.0
	Qinghai	0.69	11.20	18.70	9.88	12.37	0	16.7
	Ningxia	0.95	11.79	17.44	15.04	152.71	-9.3	-3.6
	Xinjiang	1.57	17.21	14.21	23.39	16.27	0	0
BTH	Beijing	-3.59	-6.13	9.13	5.99	-48.52	-20.4	-13.4
	Tianjin	-4.63	3.15	15.84	6.01	10.19	-9.4	-9.4
	Hebei	-5.05	4.16	12.37	6.22	10.70	-15	-12.7
YRD	Shanghai	-7.65	-0.93	6.64	0.86	-0.92	-26.9	-13.7
	Jiangsu	-5.93	5.39	12.51	7.49	13.35	-18.0	-14.8
	Zhejiang	-2.07	4.04	11.40	8.68	13.94	-15.0	-13.3
PRD	Guangdong	-4.55	6.15	12.03	5.92	6.87	-15.0	-14.8

854 a and b represents proposed reduction in SO<sub>2</sub> emission in 2010 relative to 2005, and 2015 relative  
 855 to 2010, respectively. The value for PRD refers to the proposed target for Guangdong Province.

856

857

858

859

860

861

862

863

864

865

866

867

868

869

870

871

872

873

874

875

876 **Figure Captions**

877

878 **Figure 1** Provinces, autonomous regions, and selected regions in China in this  
879 investigation. Northwestern China, defined by pink slash, includes Inner Mongolia,  
880 Shaanxi, Gansu, Qinghai, Ningxia, and Xinjiang province. Light green shadings with  
881 cross highlight Beijing-Tianjin-Hebei (BTH) and the light green color stands for the  
882 North China Plain (NCP, including BTH), including BTH, Shandong, and Henan  
883 province. The Sichuan Basin, Yangtze River Delta (YRD), and Pearl River Delta  
884 (PRD) is defined by yellow, pink, and blue color. The Urumqi-Midong region  
885 including Midong energy industrial base (MEIB) is defined by brick red. The Energy  
886 Golden Triangle (EGT), defined by purple color, including Ningdong energy  
887 chemical industrial base (NECIB) in Ningxia, Yulin in Shaanxi, and Erdos in Inner  
888 Mongolia. Red triangles indicate 188 monitoring sites across China. Blue solid  
889 circles indicate 6 selected cities in **Fig. 2**.

890

891 **Figure 2** Annually averaged  $\text{SO}_2$  VCD (DU), scaled on the right-hand-side y-axis  
892 and measured annual  $\text{SO}_2$  air concentration ( $\mu\text{g}/\text{m}^3$ ), scaled on the left-hand-side  
893 y-axis, in Beijing, Shanghai, Chongqing, Guangzhou, Yinchuan, and Urumqi.

894

895 **Figure 3** Annually averaged  $\text{SO}_2$  VCD (DU), scaled on the right-hand-side y-axis  
896 and annual emissions (thousand ton/yr) of  $\text{SO}_2$  on the left-hand-side y-axis in the  
897 NCP, YRD, PRD, Sichuan Basin, EGT, and Urumqi-Midong.

898

899 **Figure 4** Annual averaging OMI-retrieved vertical column densities of  $\text{SO}_2$  (DU)  
900 and their trends from 2005 to 2015 on  $0.25^\circ \times 0.25^\circ$  latitude/longitude resolution in  
901 China. **(a)**. Annual mean  $\text{SO}_2$  vertical column densities; **(b)**. slope (trend) of linear  
902 regression relationship between annual average OMI-retrieved  $\text{SO}_2$  VCD and the  
903 time sequence from 2005 to 2015 over China. The positive values indicate an  
904 increasing trend of  $\text{SO}_2$  VCD from 2005 to 2015, and vice versa. The blue circle  
905 highlights the six selected regions where  $\text{SO}_2$  VCD displayed dramatic change for  
906 further assessment of the long term trends and step change points in  $\text{SO}_2$  VCD.  
907 These six regions are NCP (a), YRD (b), PRD (c), Sichuan Basin (d), Energy Golden  
908 Triangle (EGT, e), and Urumqi-Midong region (f).

909

910 **Figure 5** Percentage changes in annual mean OMI  $\text{SO}_2$  VCD in the four highlighted  
911 regions in eastern and southern China and two large-scale energy industry bases in  
912 the EGT and Urumqi-Midong region in **Figure 4b** (relative to 2005).

913

914 **Figure 6** Mann-Kendall (MK) test statistics for annually  $\text{SO}_2$  VCD in those  
915 highlighted regions (**Figs. 1** and **4b**) from 2005-2015. The blue solid line is the  
916 forward sequence  $UF_k$  and the red solid line is the backward sequence  $UB_k$  defined  
917 by Eq (5). The positive values for  $UF_k$  indicate an increasing trend of  $\text{SO}_2$  VCD, and  
918 vice versa. Two straight solid lines stand for confidence interval between -1.96  
919 (straight green line) and 1.96 (straight purple line) in the MK test. The bold black  
920 line in the middle highlights zero value of  $UF_k$  and  $UB_k$ . The bold black line in the

921 middle highlights zero value of  $UF_k$  and  $UB_k$ . The intersection of  $UF_k$  and  $UB_k$   
922 sequences within the intervals between two confidence levels indicates a step change  
923 point.

924

925 **Figure 7** Annual fractions of OMI retrieved SO<sub>2</sub> VCD and emissions averaged over  
926 6 northwestern provinces in the national total SO<sub>2</sub> VCD from 2005 to 2015 and  
927 emission from 2005 to 2014. (a) fraction of annual mean SO<sub>2</sub> VCD; (b) fraction of  
928 annual mean emission. Fractions of SO<sub>2</sub> VCD are calculated as the ratio of the sum  
929 of annually averaged SO<sub>2</sub> VCD in northwestern China to the sum of annually  
930 averaged SO<sub>2</sub> VCD in the national total from 2005 to 2015 (%).

931

932 **Figure 8** Per capita SO<sub>2</sub> emission in six provinces of northwestern China and three  
933 key eastern regions (tons/person). The value for PRD refers to the per capita SO<sub>2</sub>  
934 emission for Guangdong province.

935

936 **Figure 9** Mann-Kendall (MK) test statistics for annually averaged SO<sub>2</sub> VCD in six  
937 provinces in northwestern China from 2005-2015. The blue solid line is the forward  
938 sequence  $UF_k$  and the red solid line is the backward sequence  $UB_k$  defined by Eq (5).  
939 The positive values of  $UF_k$  indicate an increasing trend of SO<sub>2</sub> VCD, and vice versa.  
940 Two straight solid lines stand for confidence interval between -1.96 (straight green  
941 line) and 1.96 (straight purple line) in the MK test. The intersection of  $UF_k$  and  $UB_k$   
942 sequences within intervals between two confidence levels indicates a step change  
943 point.

944

945 **Figure 10** Annually averaging OMI-retrieved vertical column densities of SO<sub>2</sub> (DU)  
946 in two major point sources, the MEIB in Xinjiang (a), and the NECIB in Ningxia (b).

947

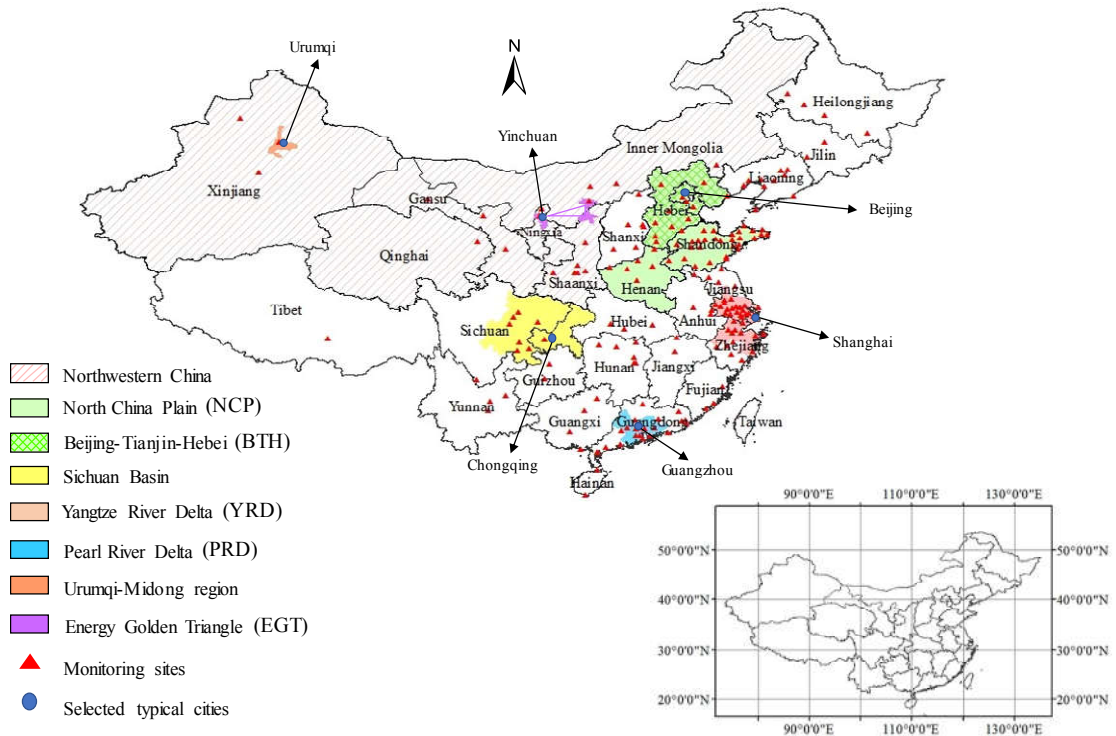
948 **Figure 11** Annually averaged SO<sub>2</sub> emissions (kt yr<sup>-1</sup>) and SO<sub>2</sub> VCD (DU) in the  
949 NECIB and MEIB, and their fractions in provincial total SO<sub>2</sub> emission and ratios  
950 between SO<sub>2</sub> VCD in these two regions and that in province. (a). SO<sub>2</sub> emission (blue  
951 bar) in the NECIB and its fraction (red solid line) in the total provincial SO<sub>2</sub>  
952 emission in Ningxia; (b). SO<sub>2</sub> emission (blue bar) in the MEIB and its fraction (red  
953 solid line) in the total provincial SO<sub>2</sub> emission in Xinjiang. (c). SO<sub>2</sub> VCD (blue bar)  
954 in the NECIB and the ratio (red solid line) between SO<sub>2</sub> VCD in the NECIB and that  
955 in Ningxia; (d). SO<sub>2</sub> VCD (blue bar) in the MEIB and the ratio (red solid line)  
956 between SO<sub>2</sub> VCD in the MEIB and that in Xinjiang; The left y-axis stands for SO<sub>2</sub>  
957 emission and the right y-axis denotes the fraction (%) at the upper panel. The left  
958 y-axis stands for SO<sub>2</sub> VCD (DU) and the right y-axis denotes the ratio at the lower  
959 panel. The error bars denotes the standard deviations of Source Detection Algorithm  
960 estimated SO<sub>2</sub> emission in two major point sources .

961

962

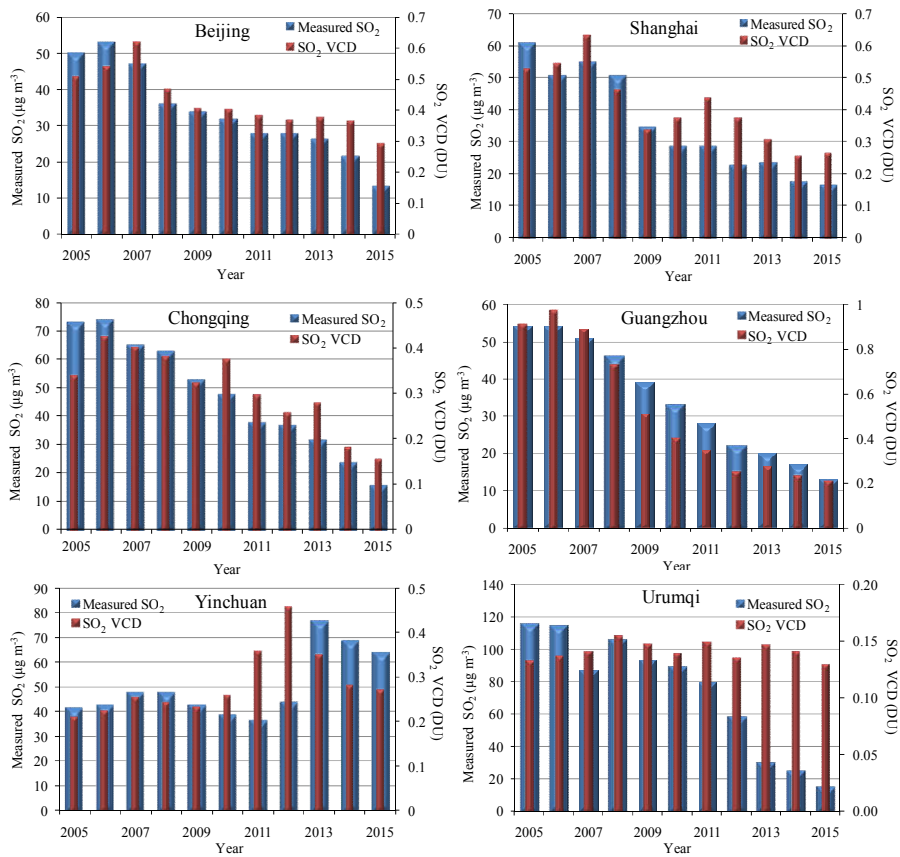
963

964 Figure 1



966  
967  
968  
969  
970  
971  
972  
973  
974  
975  
976  
977  
978  
979  
980  
981  
982  
983  
984  
985  
986  
987  
988  
989  
990

Figure 2



993

994

995

996

997

998

999

1000

1001

1002

1003

1004

1005

1006

1007

1008

1009

1010

1011

1012

1013

1014

1015

Figure 3

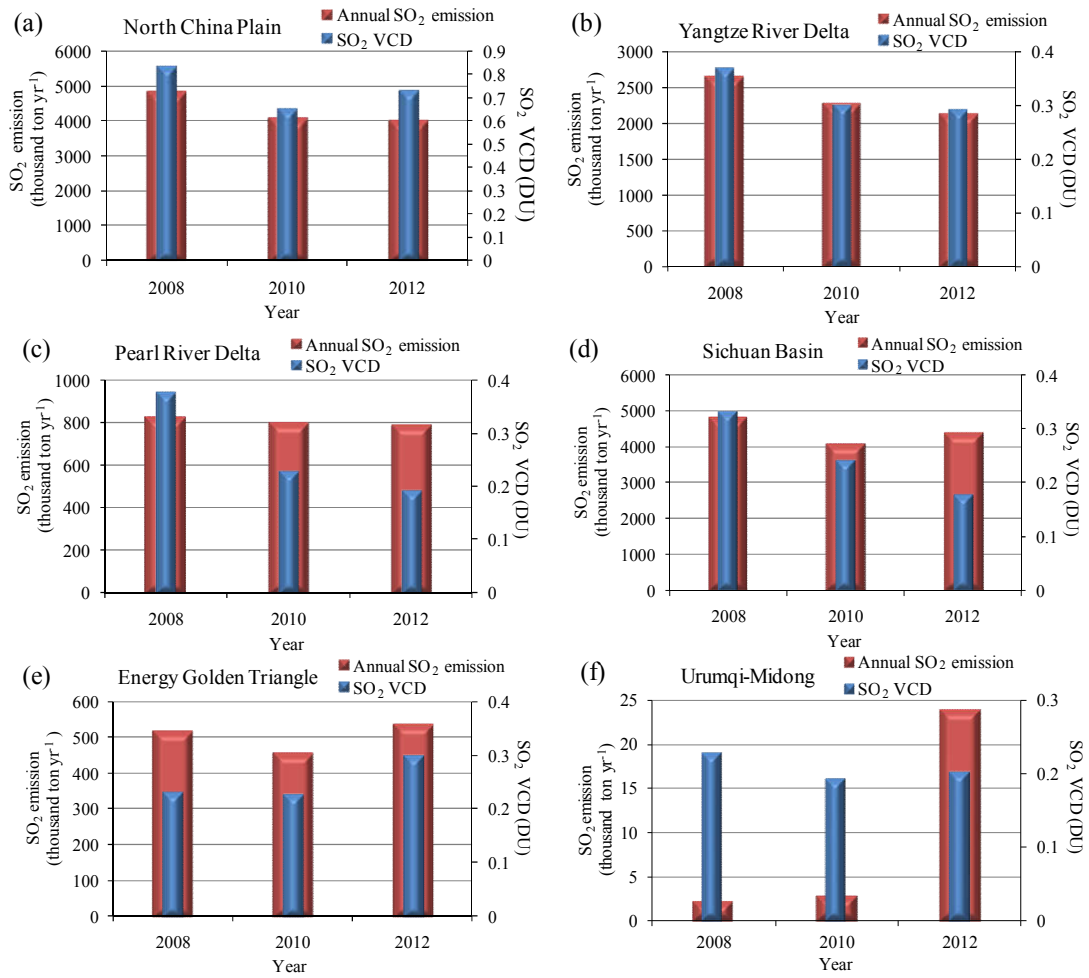
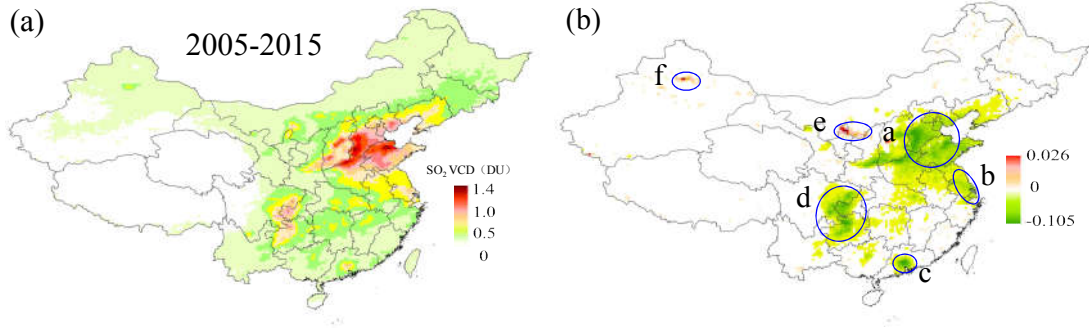


Figure 4

1037



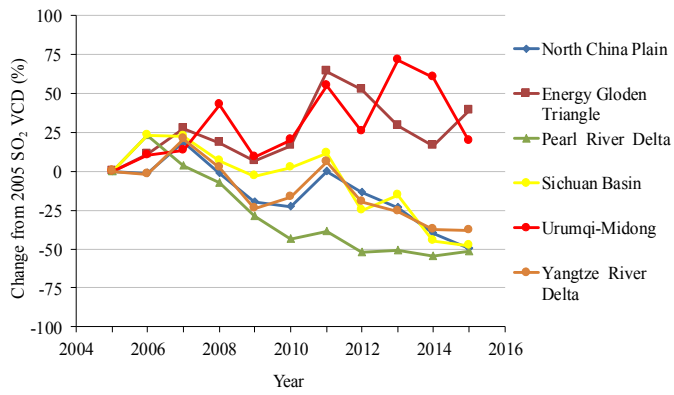
1038

1039

1040

Figure 5

1041



1042

1043

1044

1045

1046

1047

1048

1049

1050

1051

1052

1053

1054

1055

1056

1057

1058

1059

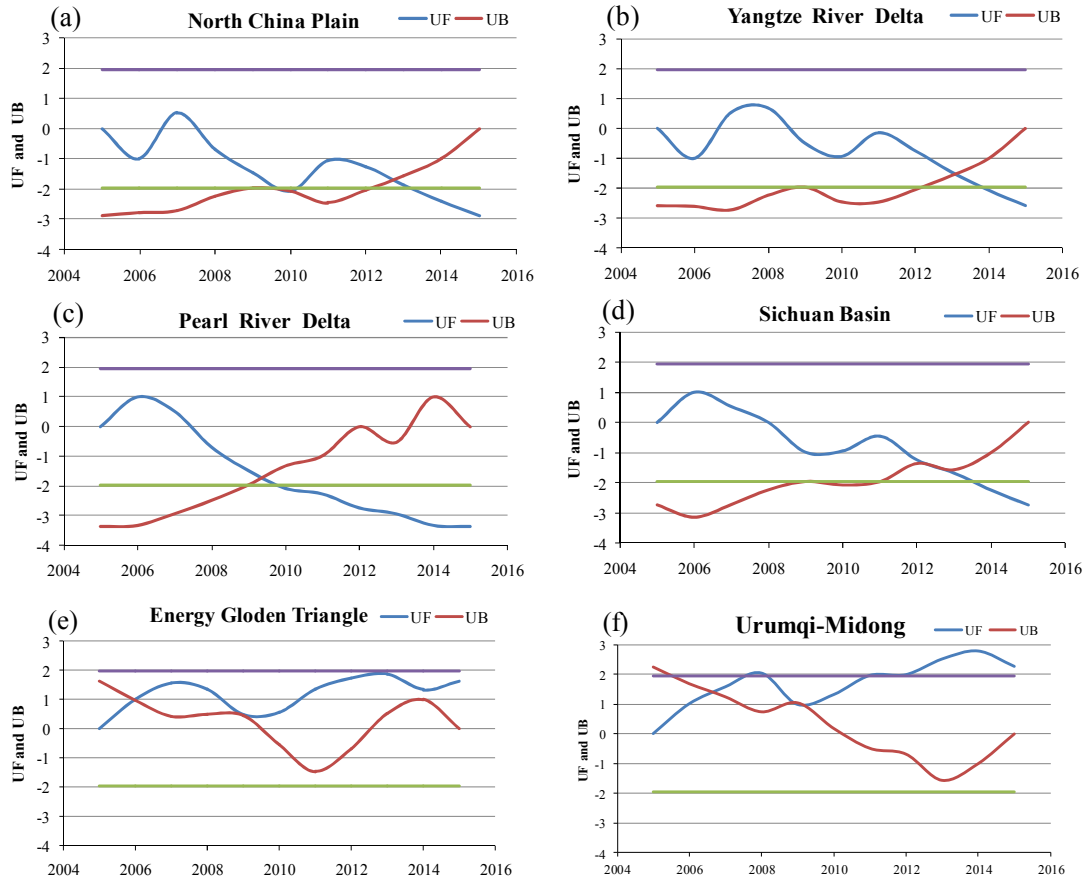
1060

1061

1062

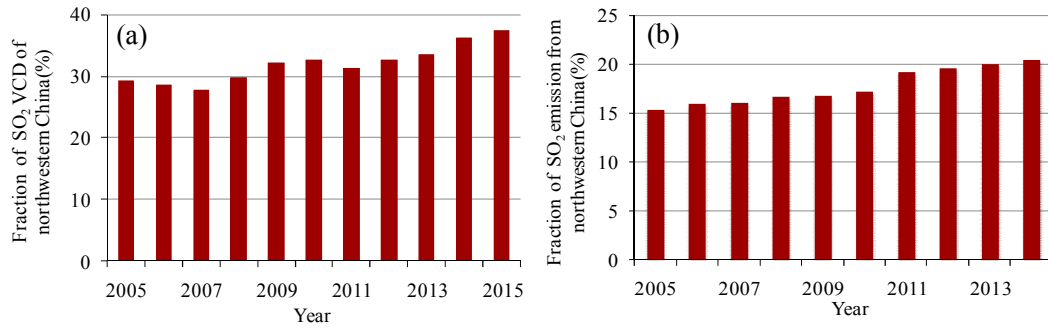
1063

Figure 6



1064  
1065  
1066  
1067

Figure 7

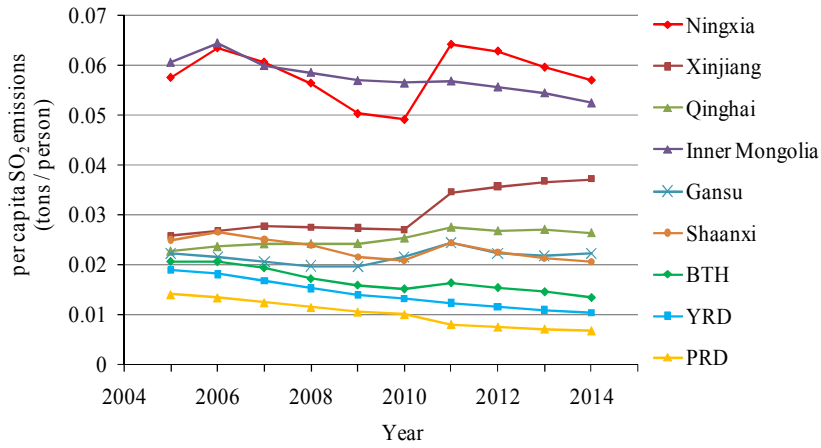


1068  
1069  
1070  
1071  
1072  
1073  
1074  
1075  
1076  
1077  
1078

Figure 8



1079

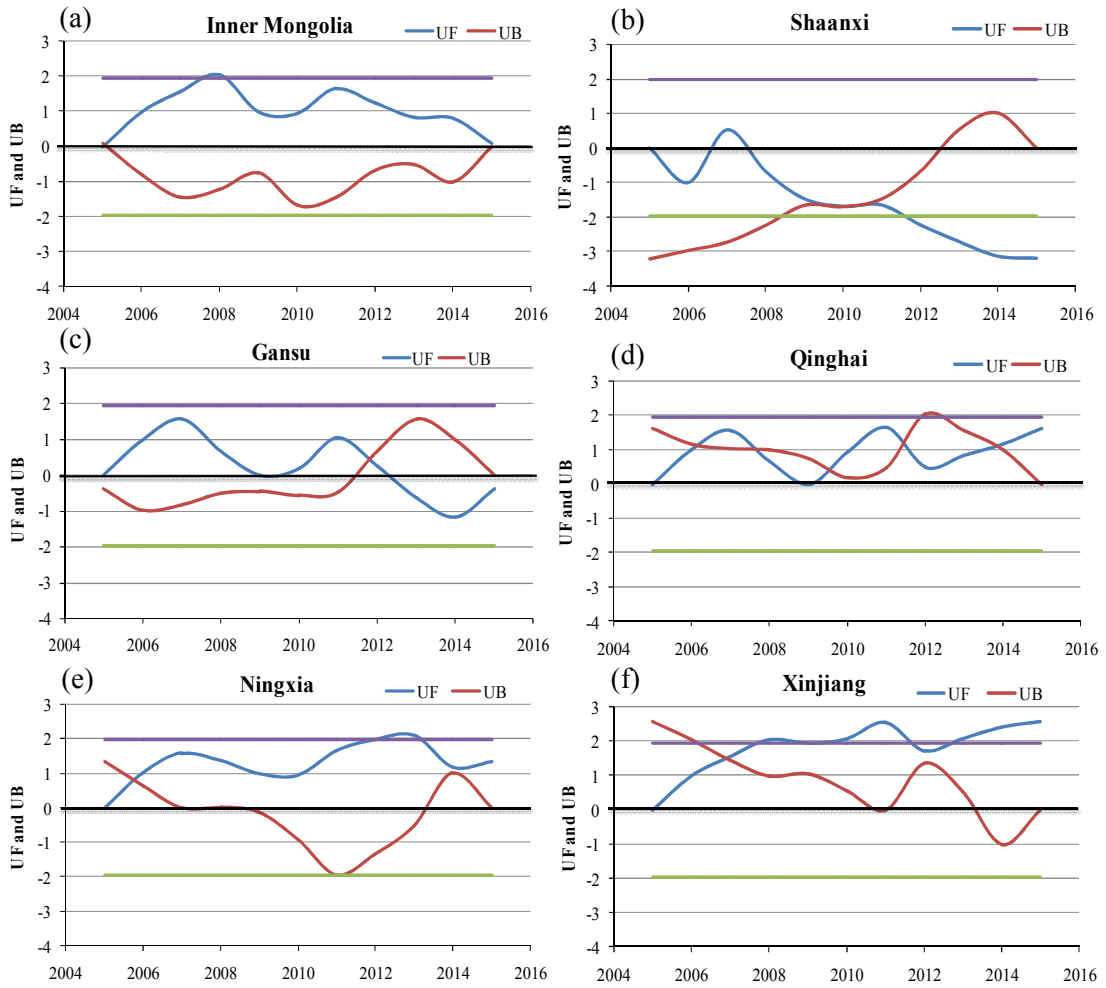


1080

1081

1082 Figure 9

1083



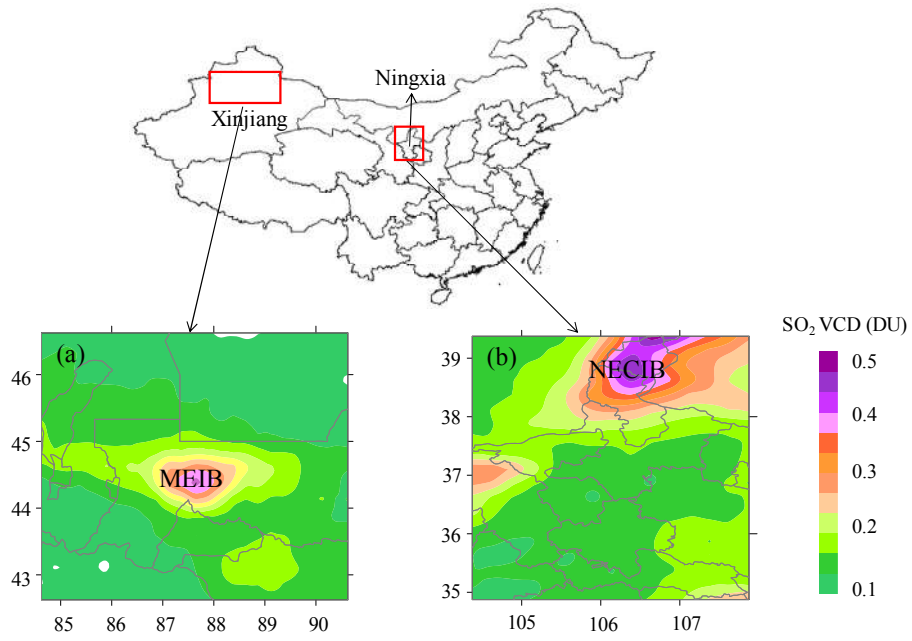
1084

1085

1086

1087 Figure 10

1088



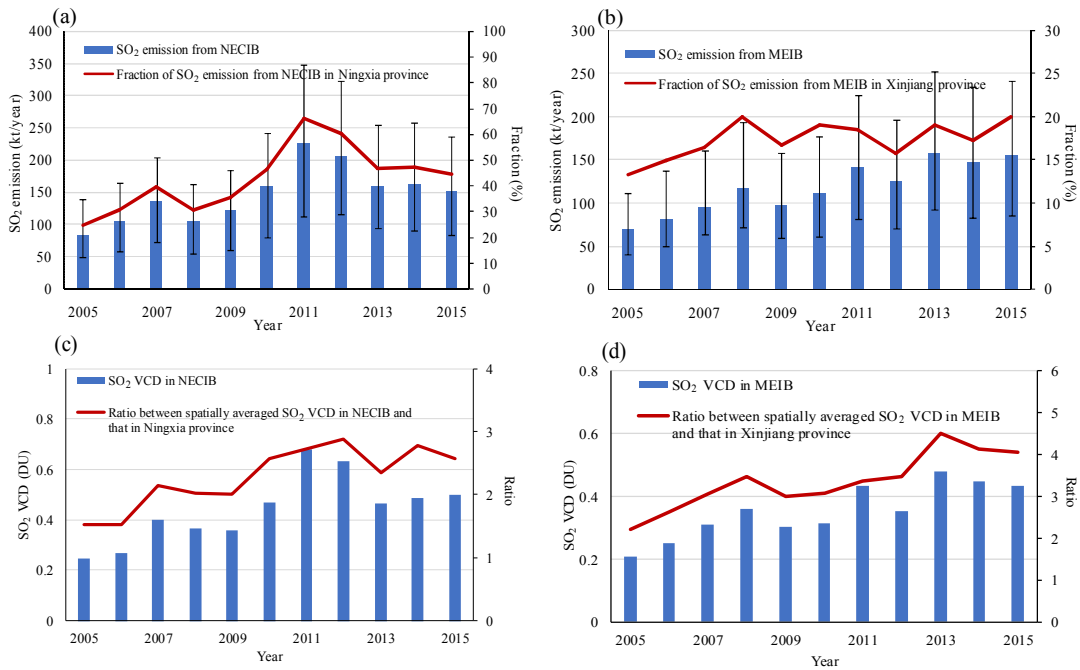
1089

1090

1091

1092 Figure 11

1093



1094